

NECOMIMI: NEURAL-COGNITIVE MULTIMODAL EEG-INFORMED IMAGE GENERATION WITH DIFFUSION MODELS

A PREPRINT

Chi-Sheng Chen

Neuro Industry, Inc.

San Francisco, CA 94114, USA

m50816m50816@gmail.com

October 2, 2024

ABSTRACT

NECOMIMI (NEural-COGnitive MultImodal EEG-Informed Image Generation with Diffusion Models) introduces a novel framework for generating images directly from EEG signals using advanced diffusion models. Unlike previous works that focused solely on EEG-image classification through contrastive learning, NECOMIMI extends this task to image generation. The proposed NERV EEG encoder demonstrates state-of-the-art (SoTA) performance across multiple zero-shot classification tasks, including 2-way, 4-way, and 200-way, and achieves top results in our newly proposed CAT Score, which evaluates the quality of EEG-generated images based on semantic concepts. A key discovery of this work is that the model tends to generate abstract or generalized images, such as landscapes, rather than specific objects, highlighting the inherent challenges of translating noisy and low-resolution EEG data into detailed visual outputs. Additionally, we introduce the CAT Score as a new metric tailored for EEG-to-image evaluation and establish a benchmark on the ThingsEEG dataset. This study underscores the potential of EEG-to-image generation while revealing the complexities and challenges that remain in bridging neural activity with visual representation.

Keywords deep learning · multimodal learning · self-supervised learning · EEG · generative model



Figure 1: This image demonstrates the capability of the NECOMIMI model to reconstruct images purely from EEG data without using the "Seen" images (ground truth) as embeddings during the generation process. The two-stage NECOMIMI architecture effectively extracts semantic information from noisy EEG signals, showing that it can capture and represent the underlying concepts from brainwave activity. The bottom row of images, generated solely from EEG input, highlights the potential of NECOMIMI to approximate the content of the "Seen" images in the top row, even in the absence of any direct visual reference or embedding.

1 Introduction

Electroencephalography (EEG) is one of the most ancient techniques used to measure neuronal activity in the human brain [1, 2]. Its application has significant value in clinical practice, particularly in diagnosing epilepsy [3], depression

[4] and sleep disorders [5], as well as in assessing dysfunctions in sensory transmission pathways [6] and more [7]. Historically, the analysis of EEG signals was limited to visual inspection of amplitude and frequency changes over time. However, with advancements in digital technology, the methodology has evolved significantly, shifting towards a more comprehensive analysis of the temporal and spatial characteristics of these signals [8]. As a result of this evolution, EEG has gained recognition as a potent tool for capturing brain functions in real-time, particularly in the sub-second range. Despite its advantages, EEG has traditionally suffered from poor spatial resolution, making it challenging to pinpoint the precise brain areas responsible for the measured neuronal activity at the scalp [9]. In recent years, there has been a surge of interest in utilizing EEG for more sophisticated applications, such as image recognition and reconstruction [10]. These advancements have led to significant improvements in the accuracy of image recognition tasks, underscoring the potential of EEG as a bridge between neural activity and visual representation [11, 12]. The growing interest in using EEG for image recognition is rooted in its ability to capture the temporal dynamics of neuronal activity, though its spatial resolution remains a challenge. Innovative methodologies, including deep learning techniques and generative models like Generative Adversarial Networks (GANs) [13] and diffusion models [14], have enhanced the accuracy and effectiveness of EEG-based systems, allowing for the generation of photorealistic images based on neural signals [12, 15, 16]. Notably, studies have demonstrated the feasibility of decoding natural images from EEG signals, employing innovative frameworks that align EEG responses with paired image stimuli [17]. However, most of the current works claiming to be EEG-to-image are essentially still image-to-image in nature, with EEG information primarily used to slightly guide the transformation of the input image by adding noise [12, 18, 19, 17]. In order to achieve a truly meaningful EEG-to-image generation, this work, named NECOMIMI (NEural-COgnitive MultiModal eeg-inforMed Image generation with diffusion models), introduces an innovative framework focused on EEG-based image generation, combining advanced diffusion model techniques.

This paper presents several key innovations as follows:

- We propose a novel EEG encoder, NERV, which achieves state-of-the-art performance in multimodal contrastive learning tasks.
- Unlike previous work that primarily focused on image-to-image generation with EEG features as guidance, we introduce a comprehensive two-stage EEG-to-image multimodal generative framework. This not only extends prior contrastive learning between EEG and images but also applies it to image generation.
- To address the conceptual differences between EEG-to-image and traditional text-to-image tasks, we propose a new quantification method, the Category-based Assessment Table (CAT) Score, which evaluates image generation performance based on semantic concepts rather than image distribution.
- We establish a CAT score benchmark standard using Vision Language Model (VLM) on the ThingsEEG dataset.
- Additionally, we uncover some notable findings and phenomena regarding the EEG-to-image generation process.

2 Related work

2.1 The potential of EEG data

In a typical experiment studying brain responses related to visual processes, a person looks at a series of images while a brain scanner or recording device captures their brain signals for analysis. There are various non-invasive methods to capture these brain responses, like fMRI, EEG, and MEG, each with different sensitivity levels. However, we still don't fully understand what this data really means, and even more importantly, how to interpret it. In a pioneering study [20], the researchers tried to generate impressions of what the subjects saw using fMRI images, based on a large image dataset taken from YouTube. However, this method has challenges, like the complexity and high cost of using an fMRI scanner. To overcome these drawbacks, a lot of research has shifted to using electrophysiological responses, particularly EEG, which has lower spatial resolution than most other methods but much higher temporal resolution. EEG recordings are also cheaper and easier to conduct, but the data is often noisy and affected by external factors, making it harder to reconstruct the original stimulus. Most image recognition and/or generation from brain signals nowadays is done using fMRI data [21], while EEG, being noisier, is used much less often.

2.2 Using EEG information on image generation and reconstruction

Building on this shift towards EEG, prior to efforts in generating images directly from brain data, the concept of using EEG signals for image classification was introduced by the study [22]. This work first demonstrated the feasibility of decoding visual categories from EEG recordings using deep learning models, setting a foundation for leveraging neural

signals in image-related tasks. However, the dataset they used was relatively small, which limited the generalization of their findings. Further advancements in generative models, specifically with the introduction of Variational Autoencoders (VAE) and Generative Adversarial Networks (GAN), opened new possibilities for image generation. The VAE model proposed by [23, 24] achieved data generation and reconstruction by learning the latent distribution of data. The GAN model introduced by [13] utilized adversarial training between a generator and a discriminator to produce highly realistic images. Building on these methods, Brain2Image [12] was the first to use VAE to guide image generation from EEG features. Following that, EEG-GAN [18] presented the first EEG-based image generation model, using LSTM [25] to extract EEG information and guide the GAN for image generation. After this, there were still many EEG-to-image works based on GAN that emerged, with most of them focusing on improving the GAN architecture and the way it interacts with the EEG encoder, like in ThoughtViz [26], VG-GAN-VC [27], BrainMedia [28], and EEG2IMAGE [16], etc. However, in all these works, a common and challenging problem is figuring out how to effectively use EEG data to guide image generation and reconstruction. This challenge of training neural networks to align multimodal information wasn't effectively addressed until the emergence of CLIP [29], which provided a much better solution. Since then, some works have also applied this approach to EEG-based image generation.

2.3 Contrastive learning-based works on EEG-image tasks

To the best of our knowledge, EEGCLIP [30] was the first to use contrastive learning to align EEG and image data. However, in this work, this aspect was only an exploratory attempt and did not further utilize the framework for downstream tasks like zero-shot image recognition. The next challenge lies in designing a better EEG encoder for contrastive learning, based on the rich image embeddings extracted from a CLIP-based image pre-trained encoder. Some recent works have explored this direction, such as NICE [31], MUSE [32], ATM [33], and [34]. Some researchers have even attempted quantum-classical hybrid computing and quantum EEG encoder [35] to perform quantum contrastive learning [36]. Most current works focus on tackling zero-shot classification, where the model is tested on unseen both EEG data and images that it hasn't encountered during training. The goal is to compute similarity scores for image recognition, aiming to enhance the model's generalization performance on out-of-sample data. As contrastive learning architectures for EEG-based image recognition mature, and inspired by test-to-image frameworks in other generative fields, the invention of diffusion models has addressed the instability issues associated with previous GAN-based generation methods to some extent. While there are already EEG-based image reconstruction efforts using diffusion models, such as NeuroVision [19], DreamDiffusion [17], DM-RE2I [37], BrainViz [38], NeuroImagen [39], and EEGVision [40], most of these works still largely rely on image-based features, with EEG data serving as supplementary information for the diffusion process. While these methods have made significant strides in computer vision, they primarily rely on images as input and are not designed to process non-visual signals like EEG directly. Currently, models designed specifically for direct generation tasks using pure EEG features or embeddings, where EEG functions similarly to a prompt command, are still quite rare. This work seeks to introduce a flexible, plug-and-play architecture: NECOMIMI, which not only expands upon previous recognition-focused approaches but also extends them into EEG-to-image generation tasks based on modern diffusion models.

3 Methodology

3.1 Overview

This chapter provides a detailed overview of an advanced EEG-to-image generation model utilizing deep learning techniques and diffusion models. While the framework includes a one-stage image generation phase, we found that its performance was suboptimal. Consequently, the model is primarily designed as a two-stage process, which will be discussed in detail in later sections. The overall structure consists of four phases: the training phase, zero-shot testing, one-stage image generation, and two-stage image generation, each contributing to the transformation of raw EEG data into meaningful visual outputs.

3.2 Training Phase

In the initial training phase, both visual image $\in \mathbb{R}^{h \times w \times ch}$ and EEG data $\in \mathbb{R}^{e \times d}$ are processed in parallel to establish a shared embedding space, where h is the height of the image, w is the width of the image, ch is the number of channels (e.g., RGB channels), e is the number of electrodes (channels), and d is the number of data points (time samples). Training set images are first passed through a pre-trained image encoder, which transforms the images into latent representations called image embeddings I . In this work, we use a pretrained Vision Transformer (ViT) [41] from CLIP model [29] as the image encoder, which outputs embeddings of size $\mathbb{R}^{1 \times 1024}$ for each image. Simultaneously, the EEG signals from the corresponding sessions are processed by a custom EEG encoder to produce EEG embeddings E . As for the EEG encoder, in this work, we extended several existing works like NICE [31], MUSE [32], Nervformer [32]

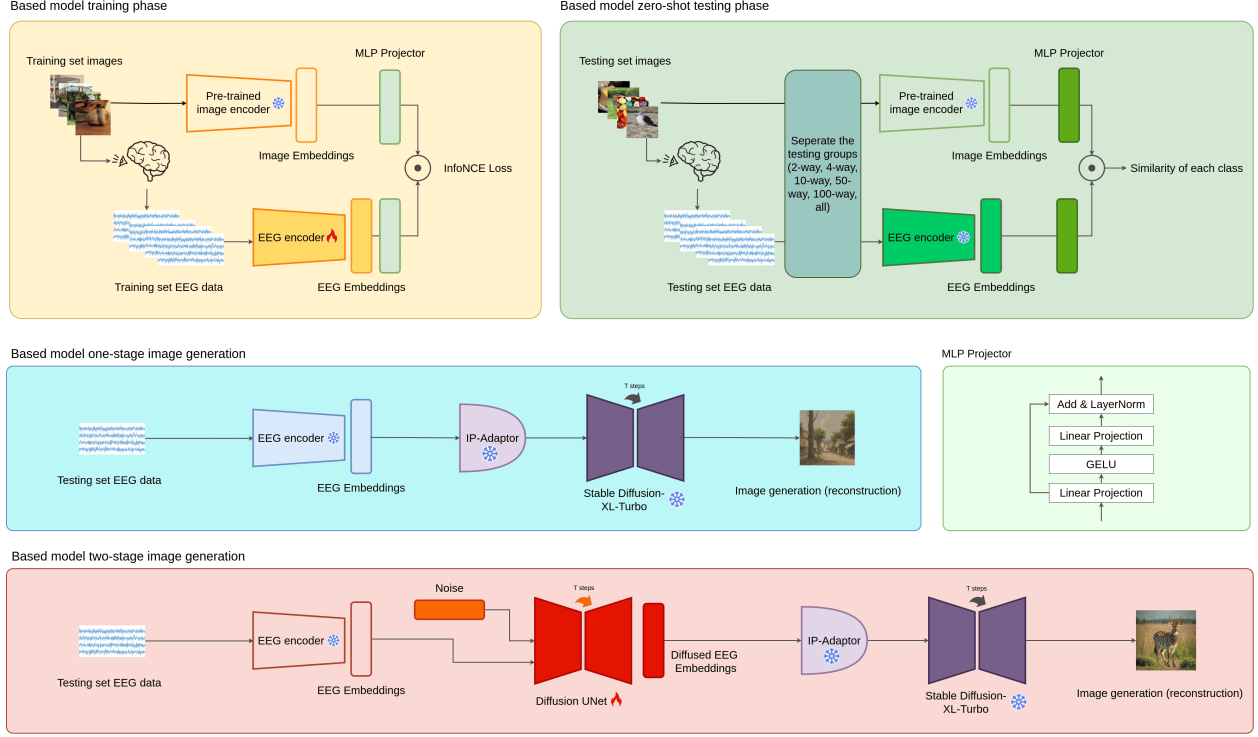


Figure 2: The figure illustrates the entire workflow of the EEG-based image generation model.

and ATM [33] to enable EEG-to-image capabilities. Additionally, we proposed a new EEG encoder, NERV, which is specifically designed for noisy, multi-channel time series data like EEG, based on a multi-attention mechanism.

These embeddings are projected into a unified space via an MLP Projector, where they are trained using the InfoNCE loss. This contrastive learning loss function ensures that corresponding image and EEG embeddings are aligned in the latent space, enhancing the model’s ability to understand and link neural patterns to visual stimuli. Standard contrastive learning employs the InfoNCE loss as defined by [42, 43, 44]:

$$\mathcal{L}_{InfoNCE} = -\mathbb{E} \left[\log \frac{\exp(S_{E,I}/\tau)}{\sum_{k=1}^N \exp(S_{E,I_k}/\tau)} \right] \quad (1)$$

where the $S_{E,I}$ represents the similarity score between the EEG embeddings E , and the paired image embeddings I , and the τ is learned temperature parameter.

3.3 Zero-shot Testing Phase

Once trained, the model enters the zero-shot testing phase. This phase focuses on evaluating the model’s ability to generalize to unseen data. Here, the EEG signals and images from the test set are encoded using the pre-trained encoders, and their respective embeddings are projected through the MLP Projector. The testing groups are separated into multiple divisions—2-way, 4-way, 10-way, 50-way, 100-way and beyond—allowing for a structured comparison between the EEG and image embeddings. The final similarity scores between embeddings determine the model’s classification accuracy, enabling the assessment of how well the model understands new EEG data without additional training.

3.4 One-stage Image Generation

In the one-stage image generation process, the EEG embeddings from the testing set are directly used as inputs to reconstruct images. By incorporating the IP-Adapter [45], which was originally designed to use images as prompts, due to its compact design, enhances image prompt flexibility within pre-trained text-to-image models. We adapt it in this work as a means to transform EEG embeddings into "feature prompts" for the image generation process. The conditioned embeddings are then processed by the Stable Diffusion XL-Turbo model [46, 47], a faster version of Stable

Diffusion XL designed for rapid image synthesis, which reconstructs the final images based on the input EEG data. This method offers a streamlined approach to EEG-based image generation, relying on a single transformation stage to produce meaningful visual outputs from neural signals. The start of the EEG-conditioned diffusion phase is critical for generating images based on EEG data. This phase uses a classifier-free guidance method, which pairs CLIP embeddings and EEG embeddings (I, E). By applying advanced generative techniques, the diffusion process is adapted to use the EEG embedding E to model the distribution of the CLIP embeddings $p(I|E)$. The CLIP embedding I , generated during this stage, lays the foundation for the next phase of image generation. The architecture integrates a simplified U-Net model, represented as $\epsilon_{\text{prior}}(I^t, t, E)$, where I^t is the noisy CLIP embedding at a specific diffusion step t .

The classifier-free guidance method helps refine the diffusion model (DM) using a specific EEG condition E . This approach synchronizes the outputs of both a conditional and an unconditional model. The final model equation is expressed as:

$$\epsilon_{\text{prior}}^w(I^t, t, E) = (1 + w)\epsilon_{\text{prior}}(I^t, t, E) - w\epsilon_{\text{prior}}(I^t, t), \quad (2)$$

where $w \geq 0$ controls the guidance scale. This technique allows for training both the conditional and unconditional models within the same network, periodically replacing the EEG embedding E with a null value to enhance training variation (about 10% of the data points). The main goal is to improve the quality of generated images while maintaining diversity.

However, we were surprised to find that when using EEG embeddings directly as prompts for the diffusion model, the generated images mostly turned out to be landscapes, regardless of the category. We will discuss the detailed results in later sections. As a result, we attempted a 2-stage approach for image generation.

3.5 Two-stage Image Generation

The prior diffusion stage plays a crucial role in generating an intermediate representation [48], such as a CLIP image embedding, from a text caption [49]. This representation is then used by the diffusion decoder to produce the final image. This two-stage process enhances image diversity, maintains photorealism, and allows for efficient and controlled image generation [50]. The two-stage image generation process introduces a more complex and refined method of synthesizing images from EEG data. In this approach, the EEG embeddings are first processed by a Diffusion U-Net, which applies additional transformations to enhance the representation of the neural data. After passing through the U-Net, the modified EEG embeddings are fed into the Stable Diffusion XL-Turbo model, with the assistance of the IP-Adaptor. This two-step transformation ensures a more nuanced generation process, potentially leading to higher-quality images by incorporating deeper layers of refinement. The first step of stage-1 is training the prior diffusion model. The main purpose of training is to let the model learn how to recover the original embedding from noisy embeddings. The specific steps are as follows: (a) Randomly replace conditional EEG embeddings c_{emb} with None with a 10% probability:

$$c_{\text{emb}} = \text{None}, \quad \text{if } \text{random}() < 0.1 \quad (3)$$

(b) Add random noise to the target embedding h_{emb} , perturb it using the scheduler at a timestep t , use the symbol $\mathcal{S}_{\text{add_noise}}$ to represent the scheduler add noise function:

$$\hat{h}_{\text{emb}}(t) = \mathcal{S}_{\text{add_noise}}(h_{\text{emb}}, \epsilon, t) \quad (4)$$

where $\epsilon \sim \mathcal{N}(0, I)$ is the random noise, and t is a randomly sampled timestep. (c) The model receives the perturbed embedding $\hat{h}_{\text{emb}}(t)$ and conditional embedding c_{emb} , and predicts the noise. Use the symbol $\mathcal{D}_{\text{prior}}$ to represent the diffusion prior function:

$$\epsilon_{\text{pred}} = \mathcal{D}_{\text{prior}}(\hat{h}_{\text{emb}}(t), t, c_{\text{emb}}) \quad (5)$$

(d) Compute the loss using Mean Squared Error (MSE) between the predicted noise and the actual noise:

$$L = \frac{1}{N} \sum_{i=1}^N \left(\epsilon_{\text{pred}}^{(i)} - \epsilon^{(i)} \right)^2 \quad (6)$$

(e) Perform backpropagation on the loss L , and update the model parameters using the optimizer:

$$\theta \leftarrow \theta - \eta \nabla_{\theta} L \quad (7)$$

where η is the learning rate and θ represents the model's parameters.

The last step of stage-1 is generation process. The main purpose of the generation process is to gradually denoise and generate the final embedding based on the conditional EEG embedding c_{emb} , starting from random noise. The

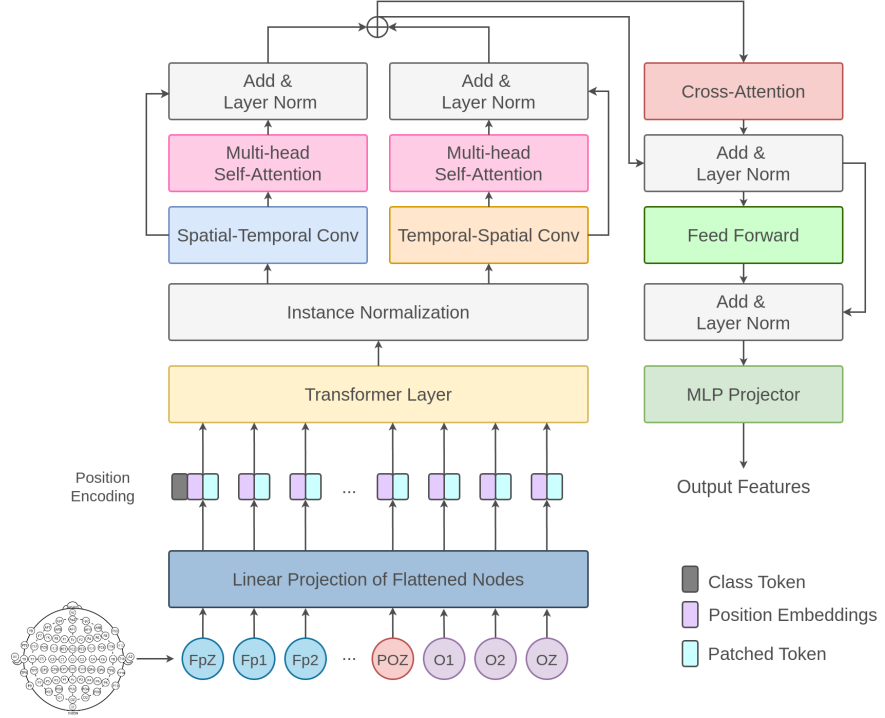


Figure 3: This diagram shows the overall structure and workflow of the NERV EEG encoder model.

specific steps are as follows: (a) Generate a sequence of timesteps t , which will be used for the denoising process, define $\mathcal{T} = \{t_1, t_2, \dots, t_T\}$ to represent the set of time steps sampled from the total steps T :

$$\{t_1, t_2, \dots, t_T\} \sim \mathcal{T}(T) \quad (8)$$

where T is the total number of denoising steps. (b) Initialize random noise embedding h_T , which serves as the starting point for the generation process:

$$h_T \sim \mathcal{N}(0, I) \quad (9)$$

(c) Starting from timestep T , iteratively apply the model to predict noise and denoise the embedding until $t = 0$. Each step depends on the conditional embedding c_{emb} :

If using conditional embedding, perform both unconditional and conditional noise prediction at each step:

$$\epsilon_{\text{pred_cond}} = \mathcal{D}_{\text{prior}}(h_t, t, c_{\text{emb}}) \quad (10)$$

$$\epsilon_{\text{pred_uncond}} = \mathcal{D}_{\text{prior}}(h_t, t) \quad (11)$$

Then combine the results using classifier-free guidance, define α_{guide} as the guidance scale:

$$\epsilon_{\text{pred}} = \epsilon_{\text{pred_uncond}} + \alpha_{\text{guide}} \times (\epsilon_{\text{pred_cond}} - \epsilon_{\text{pred_uncond}}) \quad (12)$$

Finally, update the noisy embedding based on the predicted noise, use the symbol $\mathcal{S}_{\text{step}}$ to represent the scheduler step function:

$$h_{t-1} = \mathcal{S}_{\text{step}}(\epsilon_{\text{pred}}, t, h_t) \quad (13)$$

(d) After the denoising process is complete, h_{output} represents the final generated embedding of a EEG, which is the model's output:

$$h_{\text{output}} = h_{\text{generated}} \in \mathbb{R}^{1 \times 1024} \quad (14)$$

The stage-2 is input the h_{output} into the IP-adaptor as a prompt to generate the image by Stable Diffusion XL-Turbo model.

3.6 NERV EEG Encoder

This diagram 3 illustrates the structure of NERV, a neural network encoder designed for EEG signal processing. The workflow starts with a linear projection of the flattened EEG nodes, followed by position encoding to retain temporal information. EEG signals pass through a Transformer layer and undergo instance normalization. The model then applies both spatial-temporal convolution (blue) to extract spatial features followed by temporal features and temporal-spatial convolution (yellow) to extract temporal features first, then spatial features. Multi-head self-attention mechanisms are applied to both feature sets, followed by layer normalization and residual connections. The cross-attention block (red) fuses the temporal and spatial features, which are further processed by a feed-forward layer before final output. The class token, position embeddings, and patch tokens are all part of the input sequence processed through these steps, ultimately yielding the output features for EEG-based tasks.

3.7 Category-based Assessment Table (CAT) Score

Unlike traditional image-to-image or text-to-image models driven by image representations, EEG-to-image models face unique challenges. In the current NECOMIMI architecture, the model can only capture broad semantic information from EEG signals rather than fine-grained details. For example, suppose the ground truth EEG data was recorded while a subject was observing an aircraft carrier. When using Model A as the EEG encoder in NECOMIMI, the generated image is a jet, while using Model B results in an image of a sheep. To objectively assess performance, we need a standard that scores Model A higher than Model B in such cases.

Why not use existing evaluation metrics? Traditional metrics like Structural Similarity Index (SSIM) [51] measure structural similarity between the ground truth and generated image, while the Inception Score (IS) [52] and Fréchet Inception Distance (FID) [53] focus on the accuracy of image categories and its distribution. However, EEG captures more abstract semantic information, and we cannot guarantee that the subject’s thoughts during EEG recording perfectly align with the ground truth image. This makes traditional evaluation methods unfair for EEG-to-image tasks.

To address this, we propose the Category-Based Assessment Table (CAT) Score, a new metric specifically designed for EEG-to-image evaluation. In the ThingsEEG test dataset (which contains 200 categories with one image per category), each image is manually labeled with two tags for broad categories, one for a specific category, and one for background content, resulting in a total of five tags per image. We extracted the tags by ChatGPT-4o [54]. The entire test dataset thus comprises $200 \text{ images} \times 5 \text{ tags} = 1,000$ points. Using manual annotation, we can determine whether the categories of generated images match these labels, providing a fair assessment for EEG-to-image models. For more details on the ThingsEEG categories, please refer to the appendix.

4 Experiments

4.1 Datasets and Preprocessing

The ThingsEEG dataset [55] consists of a large set of EEG recordings obtained through a rapid serial visual presentation (RSVP) paradigm. The responses were collected from 10 participants who viewed a total of 16,740 natural images from the THINGS database [56]. The dataset contains 1654 training categories, each with 10 images, and 200 test categories, each with a single image. The EEG data were recorded using 64-channel EASYCAP equipment, and preprocessing involved segmenting the data into trials from 0 to 1000 ms after the stimulus was shown, with baseline correction based on the pre-stimulus period. EEG responses for each image were averaged over multiple repetitions.

4.2 Experiment Details

Due to the significant impact that different versions of the CLIP package can have on the results of contrastive learning, this work ensures a fair comparison of various EEG encoders by rerunning all experiments using a unified CLIP-ViT environment, where available open-source code (e.g., [31]¹, [32]², [33]³) was utilized. Another factor that can influence contrastive learning is batch size. Therefore, all experiments in this work were conducted with a batch size of 1024. The final results are averaged from the best outcomes of 5 random seed training sessions, each running for 200 epochs. We employ the AdamW optimizer, setting the learning rate to 0.0002 and parameters $\beta_1=0.5$ and $\beta_2=0.999$. The τ in contrastive learning initialized with $\log(1/0.07)$. The NERV model achieves the best results with 5 multi-heads, while the Transformer layer has 1 multi-head and the cross-attention layer has 8 multi-heads. The time step is 50 in diffusion

¹<https://github.com/eyehsong/NICE-EEG>

²https://github.com/ChiShengChen/MUSE_EEG

³https://github.com/dongyangli-del/EEG_Image_decode

model. All experiments, including both EEG encoder training and prior diffusion model processing, were performed on a machine equipped with an A100 GPU.

4.3 Classification Results

In Table 1, the classification accuracy for both 2-way and 4-way zero-shot tasks is evaluated across ten subjects. Our new model NERV consistently achieves the best performance, particularly excelling in the 2-way classification task, where it maintains top accuracy across most subjects. It achieves an average accuracy of 94.8% in the 2-way classification and 86.8% in the 4-way classification, outperforming other methods like NICE [31], MUSE [32], and ATM-S [33]. While NICE and MUSE perform strongly in some subjects, they often fall short of NERV’s performance. NICE has an average of 91.3% in the 2-way task and 81.3% in the 4-way task, with MUSE trailing behind with averages of 92.2% (2-way) and 82.8% (4-way). ATM-S performs comparably to NICE and MUSE in some subjects but falls short on average with 86.5% in the 4-way classification. In Table 2, the results for the more challenging 200-way zero-shot classification task show that NERV also performs the best, especially in the top-1 accuracy. ATM-S and NERV perform similarly, but NERV shows stronger performance in most subjects. NERV achieves an average top-1 accuracy of 27.9% and top-5 accuracy of 54.7%, leading over all other methods. In contrast, Nervformer [32] and BraVL [57] show weaker performance, especially in the top-1 accuracy, where they average 19.8% and 5.8%, respectively. For the results of other 10-way, 50-way, and 100-way zero-shot classifications, please refer to the appendix. In summary, NERV consistently outperforms its competitors in both tasks, demonstrating the strongest zero-shot classification capability, particularly when distinguishing between a large number of categories, making it the most effective model in these experiments.

Table 1: Overall accuracy (%) of 2-way and 4-way zero-shot classification using CLIP-ViT as image encoder: top-1 and top-5. The parts in bold represent the best results, while the underlined parts are the second best.

Method	Subject 1		Subject 2		Subject 3		Subject 4		Subject 5		Subject 6		Subject 7		Subject 8		Subject 9		Subject 10		Ave	
	2-way	4-way	2-way	4-way																		
Subject dependent - train and test on one subject																						
Nervformer	89.9	76.9	91.3	80.7	91.6	80.8	94.3	85.9	86.3	70.4	91.1	82.5	92.5	81.6	96.2	88.3	92.0	83.7	92.4	83.1	91.8	81.4
NICE	91.7	80.4	89.8	77.4	93.5	83.7	94.0	84.9	85.9	70.3	89.1	81.7	91.2	81.7	95.8	89.2	87.9	76.5	93.8	87.1	91.3	81.3
MUSE	90.1	78.4	90.3	76.8	93.4	85.6	93.6	87.5	88.3	74.2	93.1	85.3	93.1	82.8	95.4	87.7	90.5	81.8	94.4	88.1	92.2	82.8
ATM-S	94.8	84.9	93.5	86.3	95.3	89.0	95.9	87.3	90.8	78.5	94.1	85.2	94.2	87.1	96.6	92.9	94.1	86.8	94.7	87.0	94.4	86.5
NERV (ours)	95.3	85.7	96.0	88.8	95.9	91.2	95.8	87.4	90.8	80.4	93.6	84.0	94.7	86.2	96.8	92.3	94.4	84.2	94.8	87.6	94.8	86.8

Table 2: Overall accuracy (%) of 200-way zero-shot classification using CLIP-ViT as image encoder: top-1 and top-5. The parts in bold represent the best results, while the underlined parts are the second best.

Method	Subject 1		Subject 2		Subject 3		Subject 4		Subject 5		Subject 6		Subject 7		Subject 8		Subject 9		Subject 10		Ave	
	top-1	top-5	top-1	top-5																		
Subject dependent - train and test on one subject																						
BraVL	6.1	17.9	4.9	14.9	5.6	17.4	5.0	15.1	4.0	13.4	6.0	18.2	6.5	20.4	8.8	23.7	4.3	14.0	7.0	19.7	5.8	17.5
Nervformer	15.0	36.7	15.6	40.0	19.7	44.9	23.3	54.4	13.0	29.1	18.9	42.2	19.5	42.0	30.3	60.0	20.1	46.3	22.9	47.1	19.8	44.3
NICE	19.3	44.8	15.2	38.2	23.9	51.4	24.1	51.6	11.0	30.7	18.5	43.8	21.0	47.9	32.5	63.5	18.2	42.4	27.4	57.1	21.1	47.1
MUSE	19.8	41.1	15.3	34.2	24.7	52.6	24.7	52.6	12.1	33.7	22.1	51.9	21.0	48.6	33.2	59.9	19.1	43.0	25.0	55.2	21.7	47.3
ATM-S	25.8	54.1	24.6	52.6	28.4	62.9	25.9	57.8	16.2	41.9	21.2	53.0	25.9	57.2	37.9	71.1	26.0	53.9	30.0	60.9	26.2	56.5
NERV (ours)	25.4	51.2	24.1	51.1	28.6	53.9	30.0	58.4	19.3	43.9	24.9	52.3	26.1	51.6	40.8	67.4	27.0	55.2	32.3	61.6	27.9	54.7

4.4 Performance Comparison of different generative models

Here, we introduce our newly proposed CAT Score method, which quantifies and evaluates the quality of EEG-generated images based on semantic concepts rather than pixel structure. Detailed CAT Score labels can be found in the appendix. To our surprise, while our proposed NERV method achieved SoTA on the CAT Score, no EEG encoder has surpassed a score of 500 in this evaluation out of a possible 1000 points. This highlights both the rigor of the CAT Score and the challenging nature of the pure EEG-to-Image task.

4.5 Findings in EEG-to-Image

We have observed some interesting findings from the pure EEG-to-Image process. As shown in the third row of Figure 4, the images generated by the diffusion model from embeddings compressed from EEG signals mainly consist of landscapes, which differ significantly from the original images (ground truth). Several factors may contribute to this phenomenon. For example, EEG signals are a high-noise, low-resolution form of data, capturing only certain aspects of brain activity. Moreover, we are currently unable to assess whether the brainwave data recorded from the subjects accurately captures the complete information of the original images, as the subjects might have been distracted and

Table 3: Overall CAT score $\times 1000$ of NECOMIMI EEG-to-Image generation with several EEG encoders.

	Subject 1	Subject 2	Subject 3	Subject 4	Subject 5	Subject 6	Subject 7	Subject 8	Subject 9	Subject 10	Ave
EEG Encoder	CAT Score										
Nervformer	432	457	429	454	475	463	404	438	427	410	438.9
NICE	426	456	445	447	411	454	438	443	426	429	437.5
MUSE	438	456	434	416	426	463	443	437	410	468	439.1
ATM-S	413	419	411	464	427	469	442	472	431	445	439.3
NERV (ours)	445	436	432	456	438	466	410	437	433	444	439.7



Figure 4: The image illustrates the progression of visual representations generated using different embedding techniques in a diffusion model: (a) Top row: The original images shown to subjects (ground truth). (b) Second row: Images generated by the CLIP-ViT embeddings of the original images. (c) Third row: Images generated by one-stage method using pure EEG embeddings with NERV EEG encoder. (d) Fourth row: Images generated by two-stage NECOMIMI method using pure EEG embeddings with NERV EEG encoder.

thinking about other things during the recording. This makes it difficult for the embeddings extracted from EEG signals to capture sufficient details, particularly when it comes to high-resolution object recognition (such as cats or specific items). As a result, the model tends to generate relatively vague or abstract images, like landscapes. Alternatively, the EEG signals may reflect higher-level abstract concepts or emotions associated with viewing the images rather than concrete objects or details. Since these abstract concepts are often related to the scene, background, or the brain's broad perception of the environment, the model is more likely to generate abstract or general images, such as landscapes, instead of specific objects.

Additionally, the training of the model on EEG signals may still be insufficient. The diffusion model may not yet fully understand and generate images from EEG signals, especially when it lacks enough data or optimization to map EEG signals to specific visual information. As a result, the model might more easily generate the types of images it is "accustomed" to producing, such as landscapes, which may constitute a significant portion of the training data. The gap between the vision modality and the neural modality (EEG) is also substantial. EEG signals may not directly correspond to detailed objects in images, so the model tends to generate "safe options," like landscapes, which may have been more prevalent in the image generation samples during training. This leads to what can be described as "hallucinations." These factors collectively contribute to the significant differences between the images generated from EEG signals and the ground truth, particularly the failure in specific object recognition. This work can be considered a forward-looking exploration, as this field is just beginning to develop.

5 Discussion and Conclusion

The NECOMIMI framework expands previous works on EEG-Image contrastive learning classification by enabling image generation, filling a gap in prior research and opening new possibilities for EEG applications. We introduced the SoTA EEG encoder, NERV, which achieved top performance in 2-way, 4-way, and 200-way zero-shot classification tasks, as well as in the CAT Score evaluation, demonstrating its effectiveness in EEG-based generative tasks. A key

finding is that the model often generates abstract images, like landscapes, rather than specific objects. This suggests that EEG data, being noisy and low-resolution, captures broad semantic concepts rather than detailed visuals. The gap between neural signals and visual stimuli remains a challenge for precise image generation. We also proposed the CAT Score, a new metric tailored for EEG-to-image generation, and established its benchmark on the ThingsEEG dataset. Surprisingly, we found that EEG encoder performance may not strongly correlate with the quality of generated images, providing new insights into the limitations and challenges of this task. In conclusion, NECOMIMI demonstrates the potential of EEG-to-image generation while highlighting the complexities of translating neural signals into accurate visual representations. Future research should focus on refining models to better capture detailed information from EEG signals.

Acknowledgment

I would like to thank Aidan Hung-Wen Tsai for brainstorming this fascinating title with me, which originated from a conversation in Silicon Valley about NeuroSky’s cat-ear EEG product, Necomimi. I also appreciate Neuro Industry, Inc. for providing A100 computational resources on GCP. Special thanks to Dr. Guan-Ying Chen for proofreading and providing valuable feedback on revisions.

References

- [1] Mary. The eeg in epilepsy a historical note. *Epilepsia*, 1(1-5):328–336, Jan 1959. doi:<https://doi.org/10.1111/j.1528-1157.1959.tb04270.x>. URL <https://onlinelibrary.wiley.com/doi/10.1111/j.1528-1157.1959.tb04270.x>.
- [2] David Millett. Hans berger: From psychic energy to the eeg. *Perspectives in Biology and Medicine*, 44(4):522–542, Sep 2001. doi:<https://doi.org/10.1353/pbm.2001.0070>. URL <https://muse.jhu.edu/article/26086>.
- [3] Philipp S Reif, Adam Strzelczyk, and Felix Rosenow. The history of invasive eeg evaluation in epilepsy patients. *Seizure*, 41:191–195, Apr 2016. doi:<https://doi.org/10.1016/j.seizure.2016.04.006>. URL [https://www.seizure-journal.com/article/S1059-1311\(16\)30022-X/fulltext](https://www.seizure-journal.com/article/S1059-1311(16)30022-X/fulltext).
- [4] Cheng-Ta Li, Chi-Sheng Chen, Chih-Ming Cheng, Chung-Ping Chen, Jen-Ping Chen, Mu-Hong Chen, Ya-Mei Bai, and Shih-Jen Tsai. Prediction of antidepressant responses to non-invasive brain stimulation using frontal electroencephalogram signals: Cross-dataset comparisons and validation. *Journal of Affective Disorders*, 343: 86–95, Dec 2023. doi:<https://doi.org/10.1016/j.jad.2023.08.059>. URL <https://www.sciencedirect.com/science/article/abs/pii/S0165032723010388>.
- [5] I. Hussain, Md. Azam Hossain, Rafsan Jany, Md. Azam Hossain, M. Uddin, A. Kamal, Y. Ku, and Jik-Soo Kim. Quantitative evaluation of eeg-biomarkers for prediction of sleep stages. *Sensors (Basel, Switzerland)*, 22, 2022. doi:[10.3390/s22083079](https://doi.org/10.3390/s22083079).
- [6] R. Thoma, F. Hanlon, S. Moses, J. Christopher Edgar, Mingxiong Huang, M. Weisend, J. Irwin, A. Sherwood, K. Paulson, J. Bustillo, L. Adler, Gregory A. Miller, and J. Cañive. Lateralization of auditory sensory gating and neuropsychological dysfunction in schizophrenia. *The American journal of psychiatry*, 160 9:1595–605, 2003. doi:[10.1176/APPI.AJP.160.9.1595](https://doi.org/10.1176/APPI.AJP.160.9.1595).
- [7] A. Perrottelli, G. Giordano, F. Brando, L. Giuliani, and A. Mucci. Eeg-based measures in at-risk mental state and early stages of schizophrenia: A systematic review. *Frontiers in Psychiatry*, 12, 2021. doi:[10.3389/fpsyg.2021.653642](https://doi.org/10.3389/fpsyg.2021.653642).
- [8] Louis EK;Frey. Electroencephalography (eeg): An introductory text and atlas of normal and abnormal findings in adults, children, and infants [internet], 2016. URL <https://pubmed.ncbi.nlm.nih.gov/27748095/>.
- [9] Rihui Li, Dalin Yang, Feng Fang, K. Hong, A. Reiss, and Yingchun Zhang. Concurrent fnirs and eeg for brain function investigation: A systematic, methodology-focused review. *Sensors (Basel, Switzerland)*, 22, 2022. doi:[10.3390/s22155865](https://doi.org/10.3390/s22155865).
- [10] Weijian Mai, Jian Zhang, Pengfei Fang, and Zhijun Zhang. Brain-conditional multimodal synthesis: A survey and taxonomy, 2023. URL <https://arxiv.org/abs/2401.00430>.
- [11] Concetto Spampinato, Simone Palazzo, Isaak Kavasidis, Daniela Giordano, Mubarak Shah, and Nasim Souly. Deep learning human mind for automated visual classification, 2016. URL <https://arxiv.org/abs/1609.00344>.
- [12] Isaak Kavasidis, Simone Palazzo, Concetto Spampinato, Daniela Giordano, and Mubarak Shah. Brain2image: Converting brain signals into images. In *Proceedings of the 25th ACM International Conference on Multimedia*, MM ’17, page 1809–1817, New York, NY, USA, 2017. Association for Computing Machinery. ISBN 9781450349062. doi:[10.1145/3123266.3127907](https://doi.org/10.1145/3123266.3127907). URL <https://doi.org/10.1145/3123266.3127907>.

[13] Ian J Goodfellow, Jean Pouget-Abadie, Mehdi Mirza, Bing Xu, David Warde-Farley, Sherjil Ozair, Aaron Courville, and Yoshua Bengio. Generative adversarial networks, 2014. URL <https://arxiv.org/abs/1406.2661>.

[14] Jonathan Ho, Ajay Jain, and Pieter Abbeel. Denoising diffusion probabilistic models, 2020. URL <https://arxiv.org/abs/2006.11239>.

[15] Pradeep Kumar, Rajkumar Saini, Partha Pratim Roy, Pawan Kumar Sahu, and Debi Prosad Dogra. Envisioned speech recognition using eeg sensors. *Personal and Ubiquitous Computing*, 22(1):185–199, Sep 2017. doi:<https://doi.org/10.1007/s00779-017-1083-4>. URL <https://link.springer.com/article/10.1007/s00779-017-1083-4>.

[16] Prajwal Singh, Pankaj Pandey, Krishna Miyapuram, and Shanmuganathan Raman. Eeg2image: Image reconstruction from eeg brain signals, 2023. URL <https://arxiv.org/abs/2302.10121>.

[17] Yunpeng Bai, Xintao Wang, Yan-pei Cao, Yixiao Ge, Chun Yuan, and Ying Shan. Dreamdiffusion: Generating high-quality images from brain eeg signals, 2023. URL <https://arxiv.org/abs/2306.16934>.

[18] S. Palazzo, C. Spampinato, I. Kavasidis, D. Giordano, and M. Shah. Generative adversarial networks conditioned by brain signals. In *2017 IEEE International Conference on Computer Vision (ICCV)*, pages 3430–3438, 2017. doi:[10.1109/ICCV.2017.369](https://doi.org/10.1109/ICCV.2017.369).

[19] Sanchita Khare, Rajiv Nayan Choubey, Loveleen Amar, and Venkanna Udutoalapalli. Neurovision: perceived image regeneration using crogram. *Neural Computing and Applications*, 34(8):5979–5991, Jan 2022. doi:<https://doi.org/10.1007/s00521-021-06774-1>. URL <https://link.springer.com/article/10.1007/s00521-021-06774-1>.

[20] Shinji Nishimoto, An T. Vu, Thomas Naselaris, Yuval Benjamini, Bin Yu, and Jack L. Gallant. Reconstructing visual experiences from brain activity evoked by natural movies. *Current Biology*, 21(19):1641–1646, 2011. ISSN 0960-9822. doi:<https://doi.org/10.1016/j.cub.2011.08.031>. URL <https://www.sciencedirect.com/science/article/pii/S0960982211009377>.

[21] Chenshuang Zhang, Chaoning Zhang, Mengchun Zhang, and In So Kweon. Text-to-image diffusion models in generative ai: A survey, 2023. URL <https://arxiv.org/abs/2303.07909>.

[22] C. Spampinato, S. Palazzo, I. Kavasidis, D. Giordano, N. Souly, and M. Shah. Deep learning human mind for automated visual classification. In *2017 IEEE Conference on Computer Vision and Pattern Recognition (CVPR)*, pages 4503–4511, 2017. doi:[10.1109/CVPR.2017.479](https://doi.org/10.1109/CVPR.2017.479).

[23] Diederik P Kingma and Max Welling. Auto-encoding variational bayes, 2013. URL <https://arxiv.org/abs/1312.6114>.

[24] Diederik P Kingma and Max Welling. An introduction to variational autoencoders. *Foundations and Trends® in Machine Learning*, 12(4):307–392, Jan 2019. doi:<https://doi.org/10.1561/2200000056>. URL <https://arxiv.org/abs/1906.02691>.

[25] Sepp Hochreiter and Jürgen Schmidhuber. Long short-term memory. *Neural Comput.*, 9(8):1735–1780, nov 1997. ISSN 0899-7667. doi:[10.1162/neco.1997.9.8.1735](https://doi.org/10.1162/neco.1997.9.8.1735). URL <https://doi.org/10.1162/neco.1997.9.8.1735>.

[26] Praveen Tirupattur, Yogesh Singh Rawat, Concetto Spampinato, and Mubarak Shah. Thoughtviz: Visualizing human thoughts using generative adversarial network. In *Proceedings of the 26th ACM International Conference on Multimedia*, MM ’18, page 950–958, New York, NY, USA, 2018. Association for Computing Machinery. ISBN 9781450356657. doi:[10.1145/3240508.3240641](https://doi.org/10.1145/3240508.3240641). URL <https://doi.org/10.1145/3240508.3240641>.

[27] Zhicheng Jiao, Haoxuan You, Fan Yang, Xin Li, Han Zhang, and Dinggang Shen. Decoding eeg by visual-guided deep neural networks. *Ijcai.org*, page 1387–1393, 2019. URL <https://www.ijcai.org/proceedings/2019/192>.

[28] Ahmed Fares, Sheng-hua Zhong, and Jianmin Jiang. Brain-media: A dual conditioned and lateralization supported gan (dcls-gan) towards visualization of image-evoked brain activities. In *Proceedings of the 28th ACM International Conference on Multimedia*, MM ’20, page 1764–1772, New York, NY, USA, 2020. Association for Computing Machinery. ISBN 9781450379885. doi:[10.1145/3394171.3413858](https://doi.org/10.1145/3394171.3413858). URL <https://doi.org/10.1145/3394171.3413858>.

[29] Alec Radford, Jong Wook Kim, Chris Hallacy, Aditya Ramesh, Gabriel Goh, Sandhini Agarwal, Girish Sastry, Amanda Askell, Pamela Mishkin, Jack Clark, Gretchen Krueger, and Ilya Sutskever. Learning transferable visual models from natural language supervision, 2021. URL <https://arxiv.org/abs/2103.00020>.

[30] P. Singh, D. Dalal, G. Vashishtha, K. Miyapuram, and S. Raman. Learning robust deep visual representations from eeg brain recordings. In *2024 IEEE/CVF Winter Conference on Applications of Computer Vision (WACV)*, pages 7538–7547, Los Alamitos, CA, USA, jan 2024. IEEE Computer Society. doi:[10.1109/WACV57701.2024.00738](https://doi.org/10.1109/WACV57701.2024.00738). URL <https://doi.ieee.org/10.1109/WACV57701.2024.00738>.

[31] Yonghao Song, Bingchuan Liu, Xiang Li, Nanlin Shi, Yijun Wang, and Xiaorong Gao. Decoding natural images from eeg for object recognition, 2024. URL <https://arxiv.org/abs/2308.13234>.

[32] Chi-Sheng Chen and Chun-Shu Wei. Mind's eye: Image recognition by eeg via multimodal similarity-keeping contrastive learning, 2024. URL <https://arxiv.org/abs/2406.16910>.

[33] Dongyang Li, Chen Wei, Shiyi Li, Jiachen Zou, and Quanying Liu. Visual decoding and reconstruction via eeg embeddings with guided diffusion, 2024. URL <https://arxiv.org/abs/2403.07721>.

[34] Hongzhou Chen, Lianghua He, Yihang Liu, and Longzhen Yang. Visual neural decoding via improved visual-eeg semantic consistency, 2024. URL <https://arxiv.org/abs/2408.06788>.

[35] Chi-Sheng Chen, Samuel Yen-Chi Chen, Aidan Hung-Wen Tsai, and Chun-Shu Wei. Qeegnet: Quantum machine learning for enhanced electroencephalography encoding, 2024. URL <https://arxiv.org/abs/2407.19214>.

[36] Chi-Sheng Chen, Aidan Hung-Wen Tsai, and Sheng-Chieh Huang. Quantum multimodal contrastive learning framework, 2024. URL <https://arxiv.org/abs/2408.13919>.

[37] Hong Zeng, Nianzhang Xia, Dongguan Qian, Motonobu Hattori, Chu Wang, and Wanzeng Kong. Dm-re2i: A framework based on diffusion model for the reconstruction from eeg to image. *Biomedical Signal Processing and Control*, 86:105125–105125, Sep 2023. doi:<https://doi.org/10.1016/j.bspc.2023.105125>. URL <https://www.sciencedirect.com/science/article/abs/pii/S174680942300558X?via%3Dihub>.

[38] Honghao Fu, Zhiqi Shen, Jing Jih Chin, and Hao Wang. Brainvis: Exploring the bridge between brain and visual signals via image reconstruction, 2023. URL <https://arxiv.org/abs/2312.14871>.

[39] Yu-Ting Lan, Kan Ren, Yansen Wang, Wei-Long Zheng, Dongsheng Li, Bao-Liang Lu, and Lili Qiu. Seeing through the brain: Image reconstruction of visual perception from human brain signals, 2023. URL <https://arxiv.org/abs/2308.02510>.

[40] Huangtao Guo. Eegvision: Reconstructing vision from human brain signals. *Applied Mathematics and Nonlinear Sciences*, 9(1), Jan 2024. doi:<https://doi.org/10.2478/amns-2024-1856>. URL <https://sciendo.com/article/10.2478/amns-2024-1856>.

[41] Alexey Dosovitskiy, Lucas Beyer, Alexander Kolesnikov, Dirk Weissenborn, Xiaohua Zhai, Thomas Unterthiner, Mostafa Dehghani, Matthias Minderer, Georg Heigold, Sylvain Gelly, Jakob Uszkoreit, and Neil Houlsby. An image is worth 16x16 words: Transformers for image recognition at scale, 2020. URL <https://arxiv.org/abs/2010.11929>.

[42] Aaron van den Oord, Yazhe Li, and Oriol Vinyals. Representation learning with contrastive predictive coding. *arXiv preprint arXiv:1807.03748*, 2018.

[43] Kaiming He, Haoqi Fan, Yuxin Wu, Saining Xie, and Ross Girshick. Momentum contrast for unsupervised visual representation learning. In *Proceedings of the IEEE/CVF conference on computer vision and pattern recognition*, pages 9729–9738, 2020.

[44] Alec Radford, Jong Wook Kim, Chris Hallacy, Aditya Ramesh, Gabriel Goh, Sandhini Agarwal, Girish Sastry, Amanda Askell, Pamela Mishkin, Jack Clark, et al. Learning transferable visual models from natural language supervision. In *International conference on machine learning*, pages 8748–8763. PMLR, 2021.

[45] Hu Ye, Jun Zhang, Sibo Liu, Xiao Han, and Wei Yang. Ip-adapter: Text compatible image prompt adapter for text-to-image diffusion models, 2023. URL <https://arxiv.org/abs/2308.06721>.

[46] Dustin Podell, Zion English, Kyle Lace, Andreas Blattmann, Tim Dockhorn, Jonas Müller, Joe Penna, and Robin Rombach. Sdxl: Improving latent diffusion models for high-resolution image synthesis, 2023. URL <https://arxiv.org/abs/2307.01952>.

[47] Simian Luo, Yiqin Tan, Suraj Patil, Daniel Gu, von Platen, Apolinário Passos, Longbo Huang, Jian Li, and Hang Zhao. Lcm-lora: A universal stable-diffusion acceleration module, 2024. URL <https://arxiv.org/abs/2311.05556>.

[48] Song Chun Zhu and D. Mumford. Prior learning and gibbs reaction-diffusion. *IEEE Transactions on Pattern Analysis and Machine Intelligence*, 19(11):1236–1250, 1997. doi:[10.1109/34.632983](https://doi.org/10.1109/34.632983).

[49] Aditya Ramesh, Prafulla Dhariwal, Alex Nichol, Casey Chu, and Mark Chen. Hierarchical text-conditional image generation with clip latents, 2022. URL <https://arxiv.org/abs/2204.06125>.

[50] Paul S Scotti, Atmadeep Banerjee, Jimmie Goode, Stepan Shabalin, Alex Nguyen, Ethan Cohen, Aidan J Dempster, Nathalie Verlinde, Elad Yundler, David Weisberg, Kenneth A Norman, and Tanishq Mathew Abraham. Reconstructing the mind's eye: fmri-to-image with contrastive learning and diffusion priors, 2023. URL <https://arxiv.org/abs/2305.18274>.

- [51] Zhou Wang, A.C. Bovik, H.R. Sheikh, and E.P. Simoncelli. Image quality assessment: from error visibility to structural similarity. *IEEE Transactions on Image Processing*, 13(4):600–612, 2004. doi:10.1109/TIP.2003.819861.
- [52] Tim Salimans, Ian Goodfellow, Wojciech Zaremba, Vicki Cheung, Alec Radford, and Xi Chen. Improved techniques for training gans, 2016. URL <https://arxiv.org/abs/1606.03498>.
- [53] Martin Heusel, Hubert Ramsauer, Thomas Unterthiner, Bernhard Nessler, and Sepp Hochreiter. Gans trained by a two time-scale update rule converge to a local nash equilibrium. In I. Guyon, U. Von Luxburg, S. Bengio, H. Wallach, R. Fergus, S. Vishwanathan, and R. Garnett, editors, *Advances in Neural Information Processing Systems*, volume 30. Curran Associates, Inc., 2017. URL https://proceedings.neurips.cc/paper_files/paper/2017/file/8a1d694707eb0fefe65871369074926d-Paper.pdf.
- [54] OpenAI, Josh Achiam, Steven Adler, Sandhini Agarwal, Lama Ahmad, Ilge Akkaya, Florencia Leoni Aleman, Diogo Almeida, Janko Altenschmidt, Sam Altman, Shyamal Anadkat, Red Avila, Igor Babuschkin, Suchir Balaji, Valerie Balcom, Paul Baltescu, Haiming Bao, Mohammad Bavarian, Jeff Belgum, and Irwan Bello. Gpt-4 technical report, 2023. URL <https://arxiv.org/abs/2303.08774>.
- [55] Alessandro T Gifford, Kshitij Dwivedi, Gemma Roig, and Radoslaw M Cichy. A large and rich eeg dataset for modeling human visual object recognition. *NeuroImage*, 264:119754, 2022.
- [56] Martin N Hebart, Adam H Dickter, Alexis Kidder, Wan Y Kwok, Anna Corriveau, Caitlin Van Wicklin, and Chris I Baker. Things: A database of 1,854 object concepts and more than 26,000 naturalistic object images. *PLoS one*, 14(10):e0223792, 2019.
- [57] Changde Du, Kaicheng Fu, Jinpeng Li, and Huiguang He. Decoding visual neural representations by multimodal learning of brain-visual-linguistic features. *IEEE Transactions on Pattern Analysis and Machine Intelligence*, 2023.

A Appendix

A.1 More EEG encoder classification performance comparison

Table 4: Overall accuracy (%) of 10-way zero-shot classification using CLIP-ViT as image encoder: top-1 and top-5.

Method	Subject 1	Subject 2	Subject 3	Subject 4	Subject 5	Subject 6	Subject 7	Subject 8	Subject 9	Subject 10	Ave
	10-way	10-way									
Subject dependent - train and test on one subject											
Nervformer	59.4	62.0	65.4	72.0	50.7	63.4	63.7	78.3	67.0	68.8	65.1
NICE	64.1	57.6	70.2	72.6	51.8	63.0	63.8	79.1	59.6	73.9	65.6
MUSE	61.0	56.1	70.8	71.3	55.1	70.1	66.2	76.9	62.8	73.2	66.4
ATM-S	72.5	70.4	76.3	74.1	64.6	72.2	73.6	83.2	70.6	75.8	73.3
NERV (ours)	72.2	74.3	75.9	76.7	62.5	71.8	70.4	81.8	70.9	73.8	73.0

Table 5: Overall accuracy (%) of 50-way zero-shot classification using CLIP-ViT as image encoder: top-1 and top-5.

Method	Subject 1	Subject 2	Subject 3	Subject 4	Subject 5	Subject 6	Subject 7	Subject 8	Subject 9	Subject 10	Ave
	top-1	top-5	top-1								
Subject dependent - train and test on one subject											
Nervformer	28.4	66.0	32.0	71.8	37.4	73.9	44.8	81.6	24.6	57.1	33.8
NICE	36.0	72.2	30.2	66.8	43.0	77.8	44.0	80.3	24.8	58.2	35.6
MUSE	33.9	70.9	29.9	65.7	43.6	79.4	42.8	79.8	26.1	63.4	39.8
ATM-S	45.3	78.7	44.5	80.5	49.8	85.0	46.2	83.2	33.3	69.2	42.8
NERV (ours)	41.1	74.8	43.2	80.5	47.9	82.8	48.1	83.5	36.4	70.7	43.0

Table 6: Overall accuracy (%) of 100-way zero-shot classification using CLIP-ViT as image encoder: top-1 and top-5.

Method	Subject 1	Subject 2	Subject 3	Subject 4	Subject 5	Subject 6	Subject 7	Subject 8	Subject 9	Subject 10	Ave
	top-1	top-5	top-1								
Subject dependent - train and test on one subject											
Nervformer	21.0	50.8	21.6	55.1	27.6	58.5	33.0	67.8	17.0	43.4	24.7
NICE	28.0	60.5	21.8	53.2	33.1	64.2	32.2	65.9	16.8	43.9	26.0
MUSE	25.4	56.7	21.2	49.8	33.9	67.6	32.2	65.7	18.0	49.6	30.4
ATM-S	34.9	67.7	33.1	66.9	38.1	74.3	36.0	70.2	24.6	55.6	28.4
NERV (ours)	31.1	64.4	33.1	66.9	36.6	74.1	39.0	70.2	26.1	57.1	32.9

A.2 Details of Category-based Assessment Table (CAT) Score

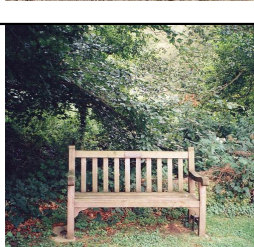
All the category-based labels are generated by ChatGPT-4o⁴, the prompt we used is "Please provide me with 5 one-word descriptions of the image, ranging from high level to low level."

Image Label	Test Image in ThingsEEG	Category-based label
00001_aircraft_carrier		Ship Island Carrier Antenna Deck
<i>Continued on next page</i>		

⁴<https://chatgpt.com>

Image Label	Test Image in ThingsEEG	Category-based label
00002_antelope		Animal Grassland Antelope Fur Horns
00003_backscratcher		Object Wood Tool Handle Backscratcher
00004_balance_beam		Structure Grass Beam Wood Support
00005_banana		Fruit Spotted Banana Plate Yellow
00006_baseball_bat		Sports Black Bats Grass Baseball
00007_basil		Plant Green Herb Leaves Basil

Continued on next page

Image Label	Test Image in ThingsEEG	Category-based label
00008_basketball		Sport Orange Basketball Ball Court
00009_bassoon		Instrument Stage Bassoon Chair Woodwind
00010_baton4		Race Yellow Relay Hand Baton
00011_batter		Cooking Whisk Batter Bowl Mixing
00012_beaver		Animal Tail Beaver Fur Paws
00013_bench		Outdoor Garden Bench Trees Wooden

Continued on next page

Image Label	Test Image in ThingsEEG	Category-based label
00014_bike		Bicycle Frame Road Path Wheels
00015_birthday_cake		Cake Frosting Flames Candles Pink
00016_blowtorch		Tool Canister Blowtorch Gas Flame
00017_boat		Boat Old Water Rowing Blue
00018_bok_choy		Vegetable Leafy BokChoy Green Stems
00019_bonnet		Hat Fabric Bonnet Vintage Ribbon

Continued on next page

Image Label	Test Image in ThingsEEG	Category-based label
00020_bottle_opener		Tool Bottlecap Opener Wooden Engraving
00021_brace		Support Black Brace Joint Strap
00022_bread		Food Slice Bread Crust Loaf
00023_breadbox		Storage Bread Breadbox Countertop Wooden
00024_bug		Insect Brown Bug Antennae Leaf
00025_buggy		Vehicle Wheels Buggy Off-road Helmet

Continued on next page

Image Label	Test Image in ThingsEEG	Category-based label
00026_bullet		Ammunition Cartridge Bullet Brass Metal
00027_bun		Food Bun Bread Round Sesame
00028_bush		Plants Mulch Bushes Shrub Green
00029_calamari		Food Plate Calamari Lemon Fried
00030_candlestick		Candlesticks Antique Brass Table Holders
00031_cart		Cart Farm Wheels Wooden Grass

Continued on next page

Image Label	Test Image in ThingsEEG	Category-based label
00032_cashew		Nuts Snack Cashews Glass
00033_cat		Animal Fur Cat Whiskers Tabby
00034_caterpillar		Insect Green Caterpillar Leaf Striped
00035_cd_player		Device Gray CDPlayer Buttons Portable
00036_chain		Metal Rusty Chain Wood Links
00037_chaps		Clothing Fringe Chaps Brown Leather

Continued on next page

Image Label	Test Image in ThingsEEG	Category-based label
00038_cheese		Food Yellow Cheese Cracker Wedge
00039_cheetah		Animal Hunt Cheetah Spotted Grassland
00040_chest2		Furniture Vintage Chest Lock Wooden
00041_chime		Instrument Metal Chime Stand Percussion
00042_chopsticks		Utensils Metal Chopsticks Case Wooden
00043_cleat		Footwear Green Cleats Studs Shoe

Continued on next page

Image Label	Test Image in ThingsEEG	Category-based label
00044_cleaver		Tool Handle Cleaver Steel Blade
00045_coat		Clothing Double-breasted Coat Black Hanger
00046_cobra		Animal Hood Cobra Sand Snake
00047_coconut		Fruit White Coconut Husk Shell
00048_coffee.Bean		Coffee Brown Beans Grinder Roasted
00049_coffeemaker		Appliance Carafe Coffeemaker Machine Buttons

Continued on next page

Image Label	Test Image in ThingsEEG	Category-based label
00050_cookie		Cookies Stack Snack Chocolate Crumb
00051_cordon_bleu		Food Breaded Chicken Stuffed CordonBleu
00052_coverall		Clothing Pockets Coverall Green Workwear
00053_crab		Animal Claws Crab Sand Beach
00054_creme_brulee		Dessert Custard CrèmeBrûlée Spoon Caramelized
00055_crepe		Dessert Banana Crepe Chocolate Plate

Continued on next page

Image Label	Test Image in ThingsEEG	Category-based label
00056_crib		Furniture Baby Crib Wooden Bedding
00057_croissant		Pastry Golden Croissant Flaky Plate
00058_crow		Bird Feathers Crow Black Beak
00059_cruise_ship		Vessel Ocean Cruise Deck Ship
00060_crumb		Crumbs Leftovers Plate White Food
00061_cupcake		Cupcake Icing Dessert Wrapper Chocolate

Continued on next page

Image Label	Test Image in ThingsEEG	Category-based label
00062_dagger		Weapon Handle Dagger Rock Blade
00063_dalmatian		Dog White Dalmatian Spotted Grass
00064_dessert		Dessert Trifle Berries Glass Cream
00065_dragonfly		Insect Striped Dragonfly Branch Wings
00066_dreidel		Toy Spinning Dreidel Letters Wooden
00067_drum		Instrument Blue Drum Percussion Sticks

Continued on next page

Image Label	Test Image in ThingsEEG	Category-based label
00068_duffel_bag		Bag Container Green Straps
00069_eagle		Bird Eagle Flight Wings Sky
00070_eel		Fish Eel Aquatic Tank Gravel
00071_egg		Eggs Bowl Brown Food Shell
00072_elephant		Animal Elephant Trunk Zoo Mammal
00073_espresso		Drink Espresso Cup Coffee Saucer

Continued on next page

Image Label	Test Image in ThingsEEG	Category-based label
00074_face_mask		Gear Cage Mask Protection Helmet
00075_ferry		Ferry Water Boat Orange Transport
00076_flamingo		Bird Water Flamingo Beach Pink
00077_folder		Folder Papers Office Desk Orange Desk
00078_fork		Utensil Plate Fork Tablecloth Silver
00079_freezer		Appliance Cold Freezer White Storage

Continued on next page

Image Label	Test Image in ThingsEEG	Category-based label
00080_french_horn		Instrument Coiled Horn Brass Shiny
00081_fruit		Fruits Colorful Assortment Fresh Tropical
00082_garlic		Garlic White Bulb Peeled Cloves
00083_glove		Gloves Wool Knitted Patterned Gray
00084_golf_cart		Vehicle Seats GolfCart White Wheels
00085_gondola		Boats Water Gondolas Blue Venice

Continued on next page

Image Label	Test Image in ThingsEEG	Category-based label
00086_goose		Bird Wings Goose Lake Flight
00087_gopher		Animal Rodent Gopher Field Furry
00088_gorilla		Animal Silverback Gorilla Primates Grass
00089_grasshopper		Insect Legs Grasshopper Antennae Green
00090_grenade		Weapon Pin Grenade Explosive Metal
00091_hamburger		Food Lettuce Hamburger Bun Grilled

Continued on next page

Image Label	Test Image in ThingsEEG	Category-based label
00092_hammer		Tool Metal Hammer Handle Claw
00093_handbrake		Automobile Lever Interior Grip Handbrake
00094_headscarf		Headwear Pink Scarf Fabric Wrap
00095_highchair		Red Highchair Wooden Furniture Chair
00096_hoodie		White Casual Hoodie Clothing Ground
00097_hummingbird		Hummingbird Small Green Bird Feeder

Continued on next page

Image Label	Test Image in ThingsEEG	Category-based label
00098_ice_cube		Ice Clear Cold Cubes Frozen
00099_ice_pack		Gel Cold Blue Cooling Reusable
00100_jeep		Off-road Adventure Rugged Durable SUV
00101_jelly_beans		Colorful Vibrant Sweet Chewy Candy
00102_jukebox		Retro Neon Vibrant Classic Music
00103_kettle		Shiny Metallic Stovetop Classic Whistling

Continued on next page

Image Label	Test Image in ThingsEEG	Category-based label
00104_kneepad		Protective Cushioned Sporty Ergonomic Durable
00105_ladle		Stainless Polished Sleek Culinary Functional
00106_lamb		Adorable Animal Fluffy Lamb Playful
00107_lampshade		Vintage Fringed Floral Ornate Fabric
00108_laundry_basket		Laundry Towels Plastic Grid Basket
00109_lettuce		Vegetable Fresh Lettuce Green Leafy

Continued on next page

Image Label	Test Image in ThingsEEG	Category-based label
00110_lightning_bug		Insect Glowing Firefly Segmented Antennae
00111_manatee		Aquatic Mammal Manatee Floating Underwater
00112_marijuana		Cannabis Leaves Plant Green Buds
00113_meatloaf		Food Sauce Meatloaf Hearty Slice
00114_metal_detector		Equipment Beach Detectors Metal Lineup
00115_minivan		Vehicle Blue Minivan Electric Car

Continued on next page

Image Label	Test Image in ThingsEEG	Category-based label
00116_modem		Device Black Modem Connectivity Router
00117_mosquito		Insect Legs Mosquito Proboscis Biting
00118_muff		Accessory Warm Muff Fur Pink
00119_music_box		Device Crank Music Punched Box
00120_mussel		Seafood Steamed Mussels Parsley Shells
00121_nightstand		Furniture Drawer Nightstand Lamp Wooden

Continued on next page

Image Label	Test Image in ThingsEEG	Category-based label
00122_okra		Vegetable Basket Okra Green Fresh
00123_omelet		Breakfast Tomatoes Omelet Vegetables Herbs
00124_onion		Vegetable Sliced Onion Red Raw
00125_orange		Fruit Sliced Orange Juicy Citrus
00126_orchid		Flower Bloom Orchid Yellow Petals
00127_ostrich		Bird Plumage Ostrich Large Road

Continued on next page

Image Label	Test Image in ThingsEEG	Category-based label
00128_pajamas		Clothing Blue Pajamas Striped Fabric
00129_panther		Animal Predator Panther Black Stealthy
00130_paperweight		Office Eyeball Paperwork Documents Paperweight
00131_pear		Fruit Green Pear Ripe Tree
00132_pepper1		Spice Black Pepper Spoon Ground
00133_pheasant		Bird Colorful Pheasant Wild Feathers

Continued on next page

Image Label	Test Image in ThingsEEG	Category-based label
00134_pickax		Tool Metal Pickaxe Wooden Digging
00135_pie		Dessert Crust Pie Golden Baked
00136_pigeon		Bird Perched Pigeon Grey Feathers
00137_piglet		Animal Grass Piglet Spotted Cute
00138_pocket		Clothing Denim Jeans Stitched Pocket
00139_pocketknife		Tool Compact Pocketknife Multi-functional Blade

Continued on next page

Image Label	Test Image in ThingsEEG	Category-based label
00140_popcorn		Snack Buttery Popcorn Crispy Bowl
00141_popsicle		Dessert Frozen Popsicle Colorful Fruit
00142_possum		Animal Marsupial Possum Furry Wild
00143_pretzel		Snack Baked Pretzel Salted Dough
00144_pug		Animal Leash Pug Panting Dog
00145_punch2		Tool Office Punch Metal Desk

Continued on next page

Image Label	Test Image in ThingsEEG	Category-based label
00146_purse		Accessory Green Purse Handles
00147_radish		Vegetable Fresh Radish Bunch
00148_raspberry		Fruit Berry Raspberry Branch
00149_recorder		Instrument Notes Recorder Music Sheet
00150_rhinoceros		Animal Savanna Rhinoceros Wild Horned
00151_robot		Robot Black White Toy Humanoid

Continued on next page

Image Label	Test Image in ThingsEEG	Category-based label		
00152_rooster		Bird Colorful	Rooster Comb	Feathers
00153_rug		Furniture Red	Rug Ornate	Patterned
00154_sailboat		Boat White	Sailboat Wind	Ocean
00155_sandal		Footwear Straps	Sandals Brown	Leather
00156_sandpaper		Tool Roll	Sandpaper Rough	Abrasive
00157_sausage		Food Smoked	Sausage Meat	Sliced

Continued on next page

Image Label	Test Image in ThingsEEG	Category-based label
00158_scallion		Vegetable Fresh Scallion Green Bundle
00159_scallop		Seafood Plate Scallops Garnish Seared
00160_scooter		Vehicle Green Scooter Urban Electric
00161_seagull		Bird White Seagull Walking Beach
00162_seaweed		Marine Aquatic Seaweed Sunlight Underwater
00163_seed		Food Brown Seeds Spoon Flax

Continued on next page

Image Label	Test Image in ThingsEEG	Category-based label
00164_skateboard		Sport Outdoor Skateboard Wheels Deck
00165_sled		Winter Snow Sled Wooden Sleigh
00166_sleeping_bag		Camping Outdoor Sleeping Bag Frost
00167_slide		Playground Ladder Slide Blue Outdoor
00168_slingshot		Tool Rubber Slingshot Wooden Y-shaped
00169_snowshoe		Footwear Running Snowshoes Yellow Winter

Continued on next page

Image Label	Test Image in ThingsEEG	Category-based label
00170_spatula		Utensil Slotted Spatula Metal Handle
00171_spoon		Utensil Reflection Spoon Curved Metal
00172_station_wagon		Vehicle Red Station Classic Wagon
00173_stethoscope		Medical Black Stethoscope Diagnosis Instrument
00174_strawberry		Fruit Ripe Strawberry Plant Red
00175_submarine		Vessel Water Submarine Stealth Navy

Continued on next page

Image Label	Test Image in ThingsEEG	Category-based label
00176_suit		Clothing Business Suit Tailored Formal
00177_t-shirt		Clothing Event T-shirt Hanger White
00178_table		Furniture Square Table Drawer Wooden
00179_taillight		Vehicle Classic Taillight Chrome Pink
00180_tape_recorder		Device Vintage Recorder Audio Cassette
00181_television		Electronics Screen Television Retro CRT

Continued on next page

Image Label	Test Image in ThingsEEG	Category-based label
00182_tiara		Crown Jewels Tiara Gold Red
00183_tick		Insect Skin Tick Parasite Tiny
00184_tomato_sauce		Food Pot Sauce Tomato Red
00185_tongs		Utensil Grip Tongs Metal Kitchen
00186_tool		Tools Screwdriver Hammer Pliers Utility
00187_top_hat		Accessory Gloves Top-hat Velvet Cane

Continued on next page

Image Label	Test Image in ThingsEEG	Category-based label
00188_treadmill		Exercise Indoor Treadmill Machine Fitness
00189_tube_top		Clothing Yellow Top Striped Knitted
00190_turkey		Bird Fanned Turkey Feathers Brown
00191_unicycle		Vehicle Tire Unicycle Wheel Seat
00192_vise		Tool Clamp Vise Adjustable Metal
00193_volleyball		Sport Ball Volleyball Beach Sand

Continued on next page

Image Label	Test Image in ThingsEEG	Category-based label
00194_wallpaper		Interior Vintage Wallpaper Pattern Wood
00195_walnut		Food Shell Walnut Brown Nut
00196_wheat		Crop Field Wheat Stalk Grain
00197_wheelchair		Mobility Wheels Wheelchair Manual Seat
00198_windshield		Vehicle Car Windshield Street Glass
00199_wine		Beverage Grapes Wine Red Glass

Continued on next page

Image Label	Test Image in ThingsEEG	Category-based label
00200_wok		Cookware Handles Wok Black Pan

B The image generation results of NECOMIMI

In this section, we will present all the images generated by various EEG encoders within the NECOMIMI framework using a fixed random seed. These images are generated using the testing set of the ThingsEEG dataset in a zero-shot setting, meaning that the model has not seen these categories during the EEG-Image contrastive learning training process. All the images illustrate the progression of visual representations generated using different embedding techniques in a diffusion model: (a) Top row: The original images shown to subjects (ground truth). (b) Second row: Images generated by the CLIP-ViT embeddings of the original images. It is only related to the seed and has nothing to do with the subject and EEG encoder. (c) Third row: Images generated by one-stage method using pure EEG embeddings with the EEG encoder. (d) Fourth row: Images generated by two-stage NECOMIMI method using pure EEG embeddings with EEG encoder.

B.1 Using NICE as the EEG encoder

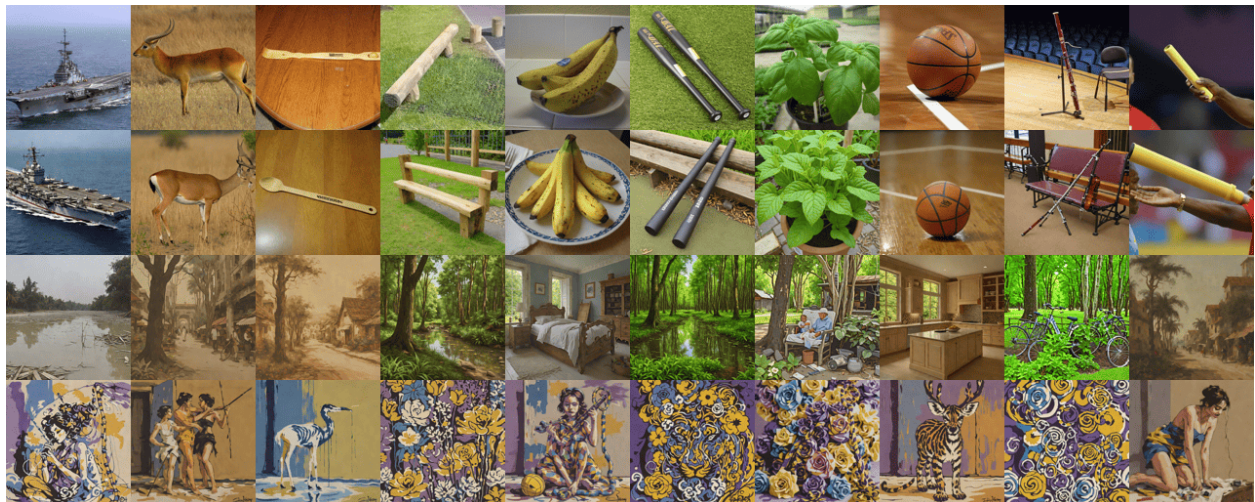


Figure 5: Random selected generated images in Subject 6 with NICE EEG encoder.



Figure 6: Random selected generated images in Subject 6 with NICE EEG encoder.

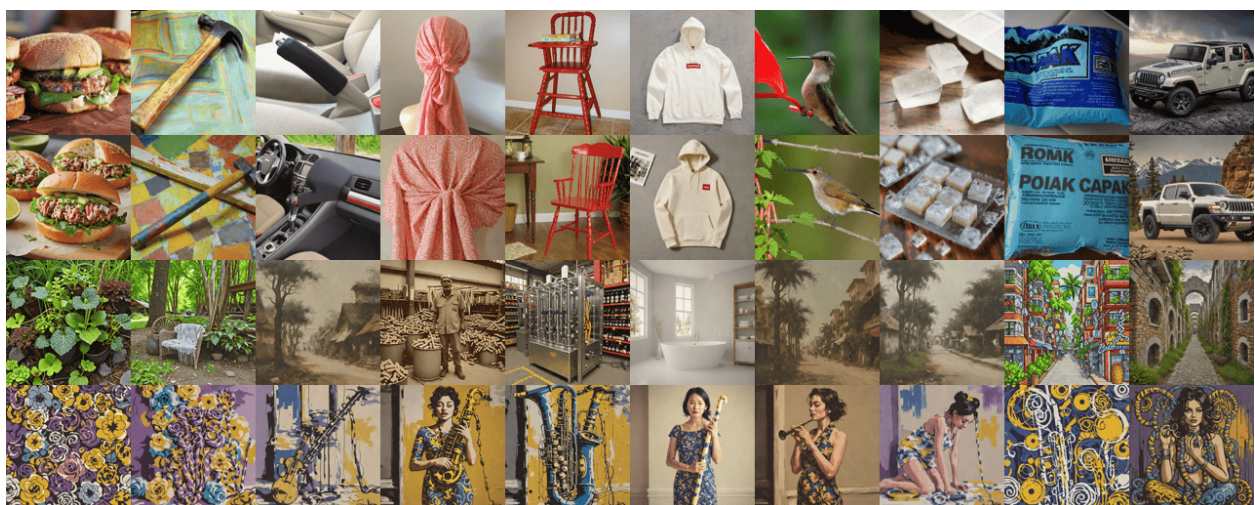


Figure 7: Random selected generated images in Subject 6 with NICE EEG encoder.



Figure 8: Random selected generated images in Subject 7 with NICE EEG encoder.

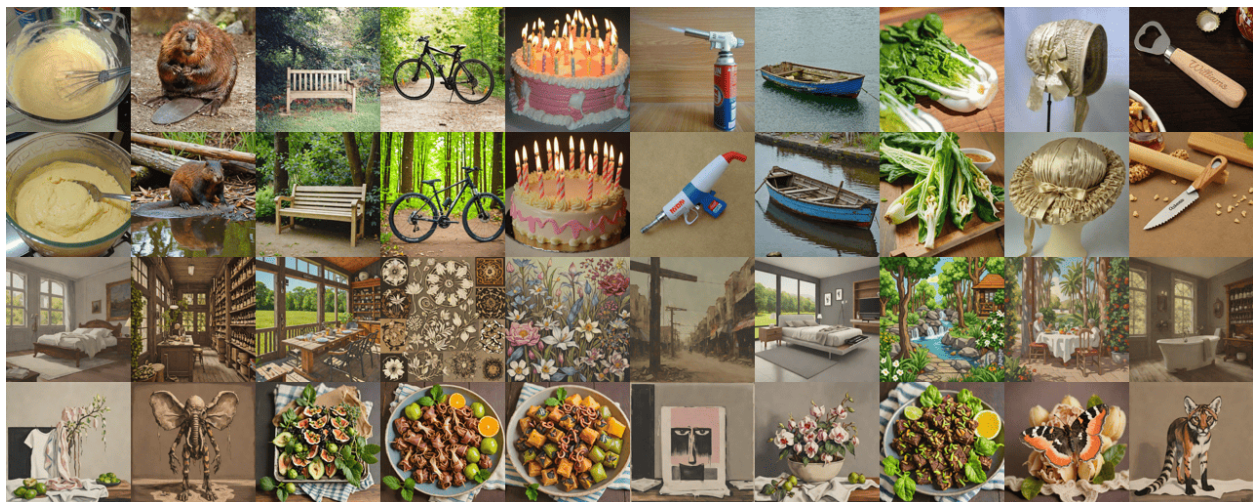


Figure 9: Random selected generated images in Subject 7 with NICE EEG encoder.

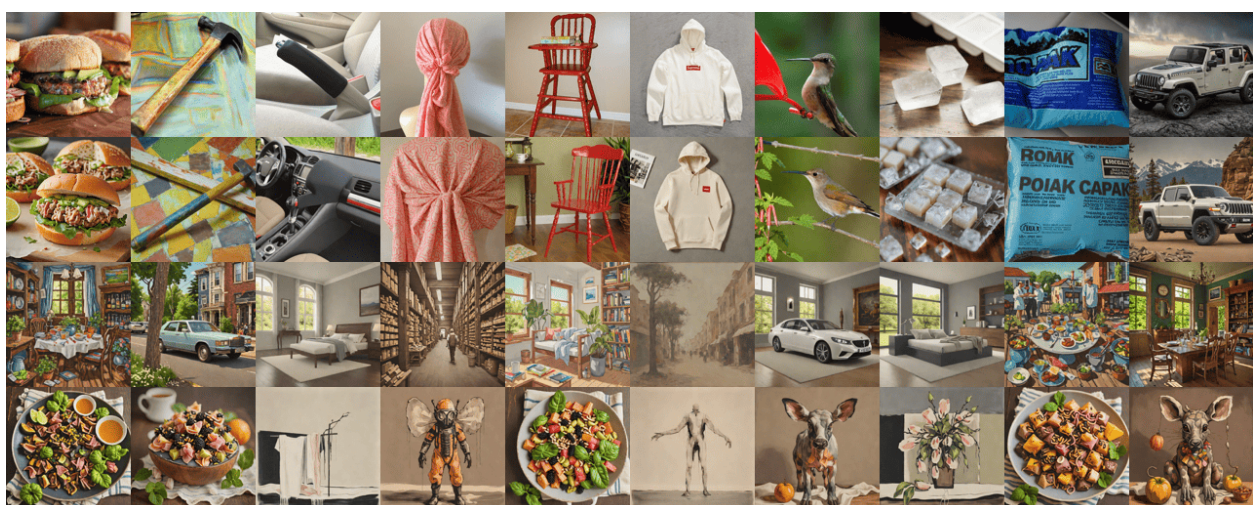


Figure 10: Random selected generated images in Subject 7 with NICE EEG encoder.



Figure 11: Random selected generated images in Subject 8 with NICE EEG encoder.



Figure 12: Random selected generated images in Subject 8 with NICE EEG encoder.

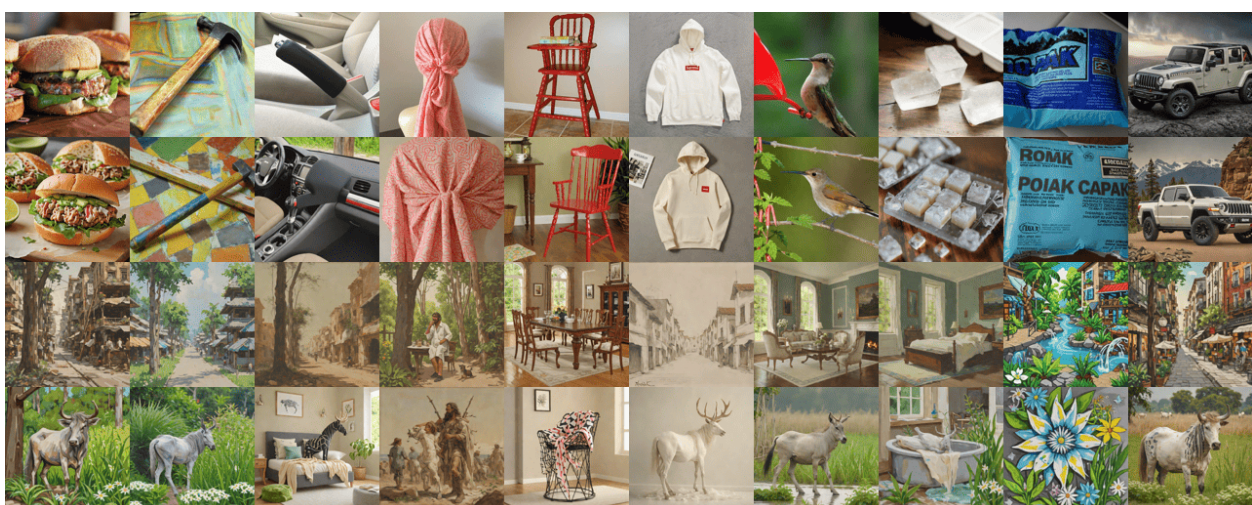


Figure 13: Random selected generated images in Subject 8 with NICE EEG encoder.



Figure 14: Random selected generated images in Subject 6 with Nervformer EEG encoder.



Figure 15: Random selected generated images in Subject 6 with Nervformer EEG encoder.



Figure 16: Random selected generated images in Subject 6 with Nervformer EEG encoder.

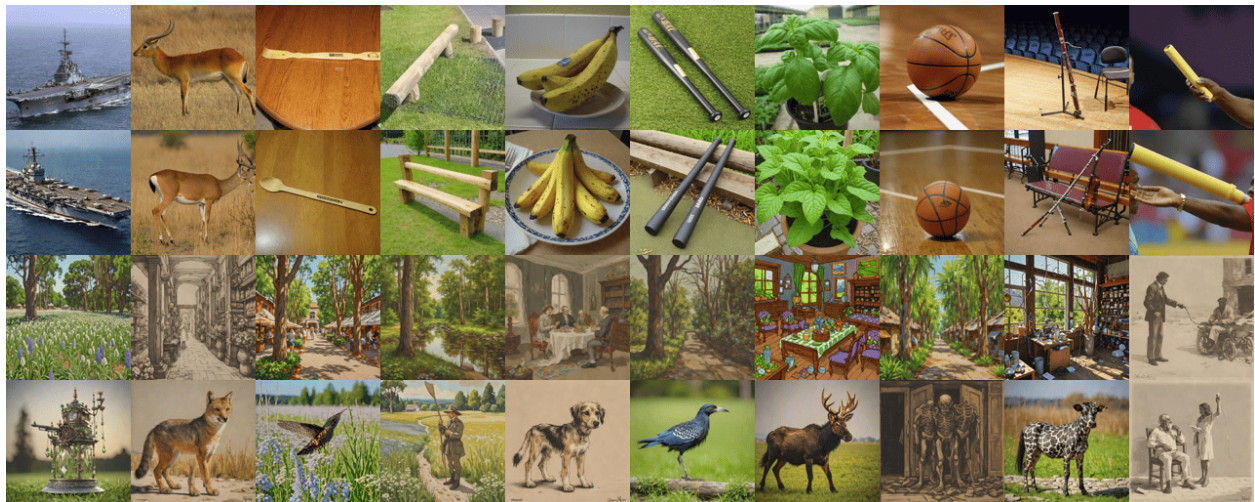


Figure 17: Random selected generated images in Subject 7 with Nervformer EEG encoder.



Figure 18: Random selected generated images in Subject 7 with Nervformer EEG encoder.

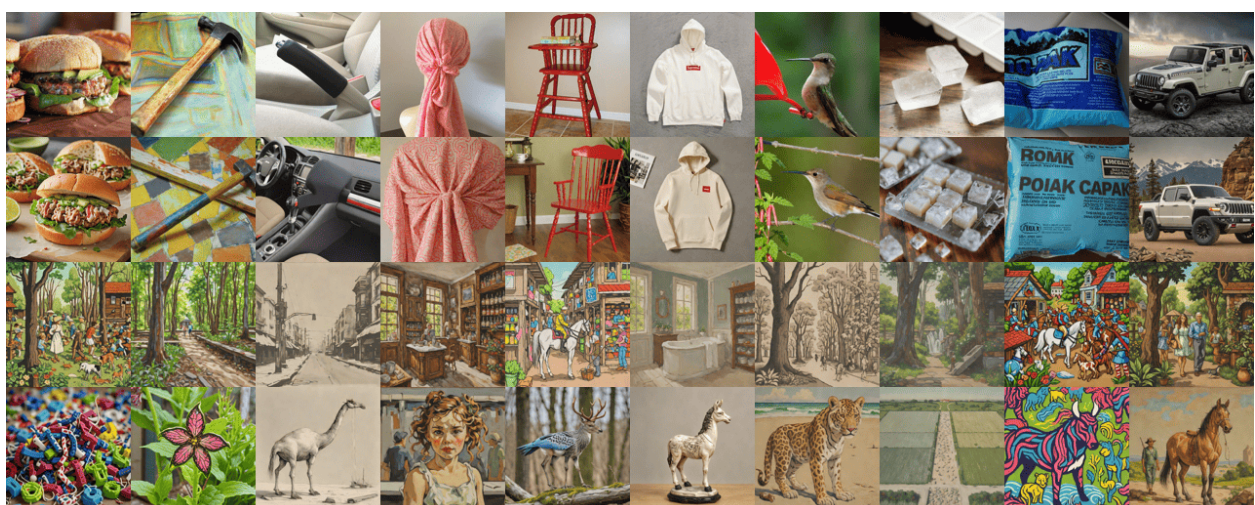


Figure 19: Random selected generated images in Subject 7 with Nervformer EEG encoder.



Figure 20: Random selected generated images in Subject 8 with Nervformer EEG encoder.

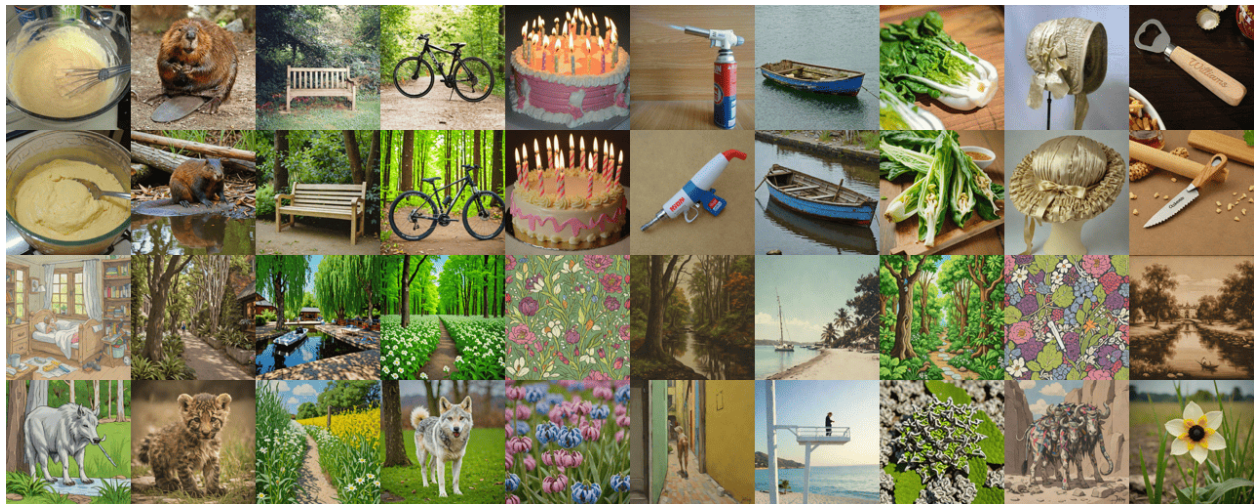


Figure 21: Random selected generated images in Subject 8 with Nervformer EEG encoder.



Figure 22: Random selected generated images in Subject 8 with Nervformer EEG encoder.



Figure 23: Random selected generated images in Subject 6 with MUSE EEG encoder.

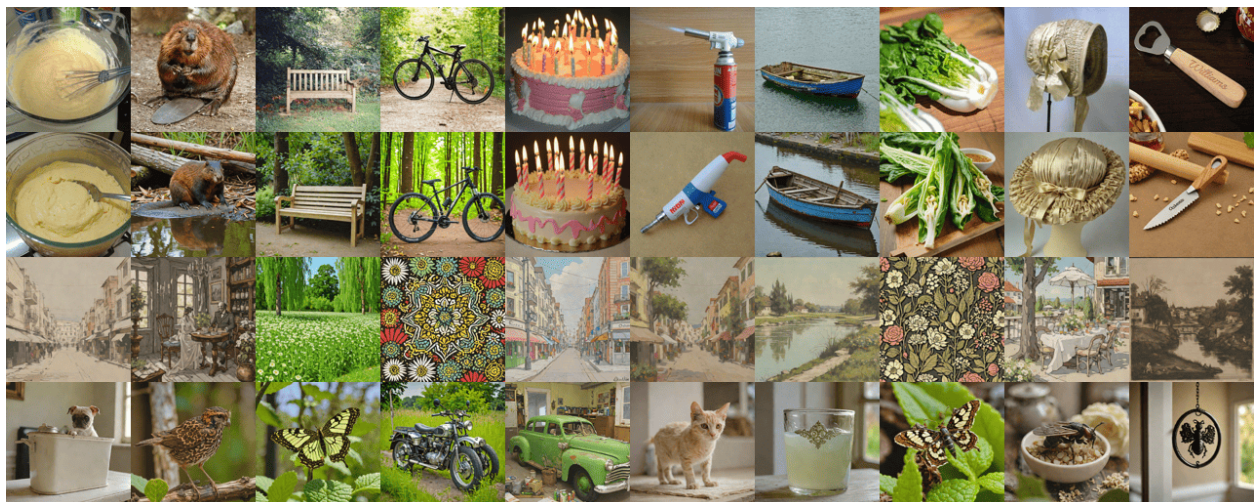


Figure 24: Random selected generated images in Subject 6 with MUSE EEG encoder.



Figure 25: Random selected generated images in Subject 6 with MUSE EEG encoder.

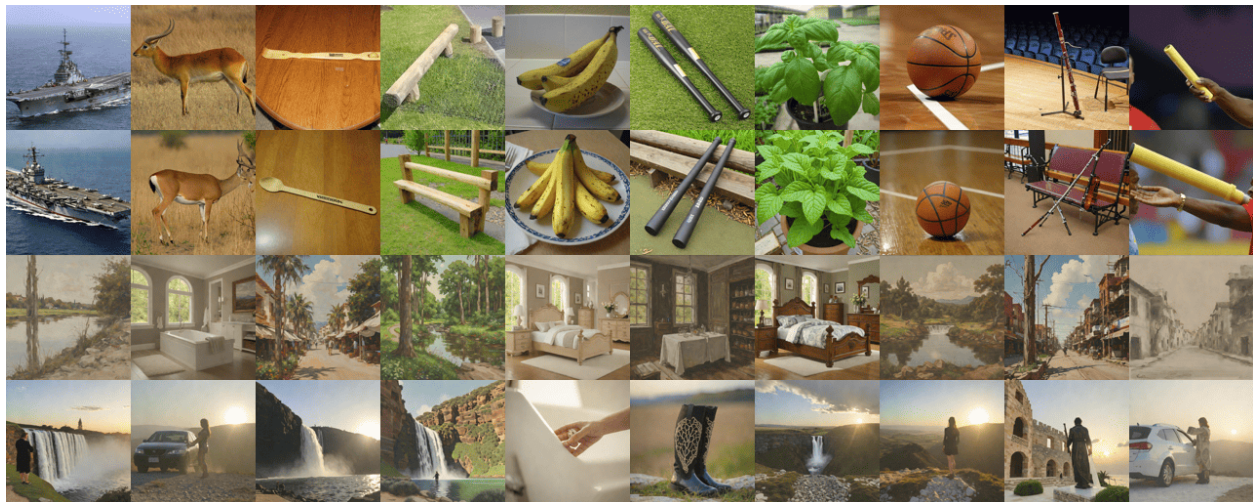


Figure 26: Random selected generated images in Subject 7 with MUSE EEG encoder.

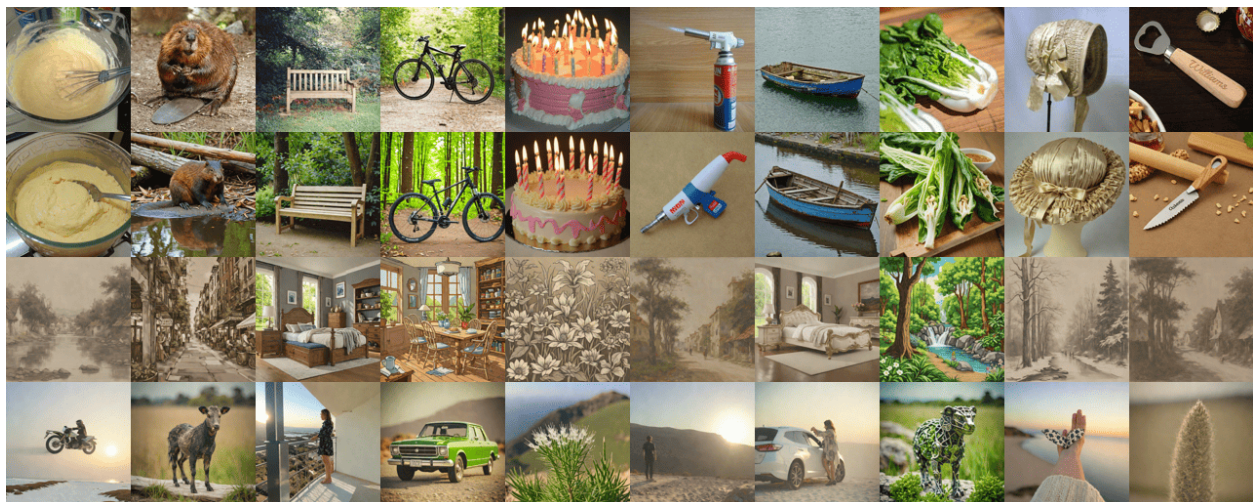


Figure 27: Random selected generated images in Subject 7 with MUSE EEG encoder.



Figure 28: Random selected generated images in Subject 7 with MUSE EEG encoder.



Figure 29: Random selected generated images in Subject 8 with MUSE EEG encoder.



Figure 30: Random selected generated images in Subject 8 with MUSE EEG encoder.



Figure 31: Random selected generated images in Subject 8 with MUSE EEG encoder.

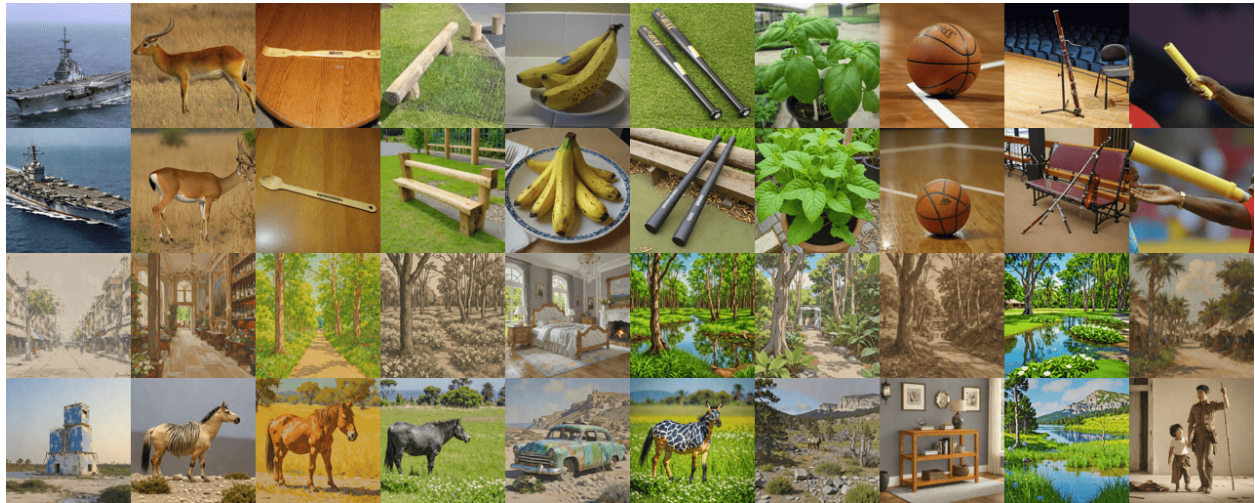


Figure 32: Random selected generated images in Subject 6 with ATM-S EEG encoder.



Figure 33: Random selected generated images in Subject 6 with ATM-S EEG encoder.

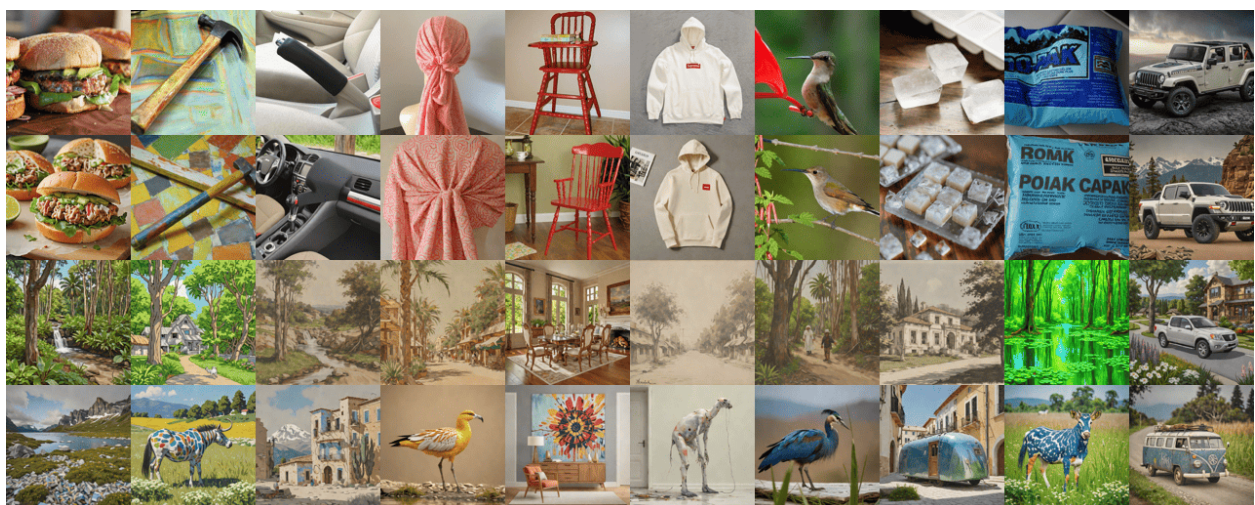


Figure 34: Random selected generated images in Subject 6 with ATM-S EEG encoder.

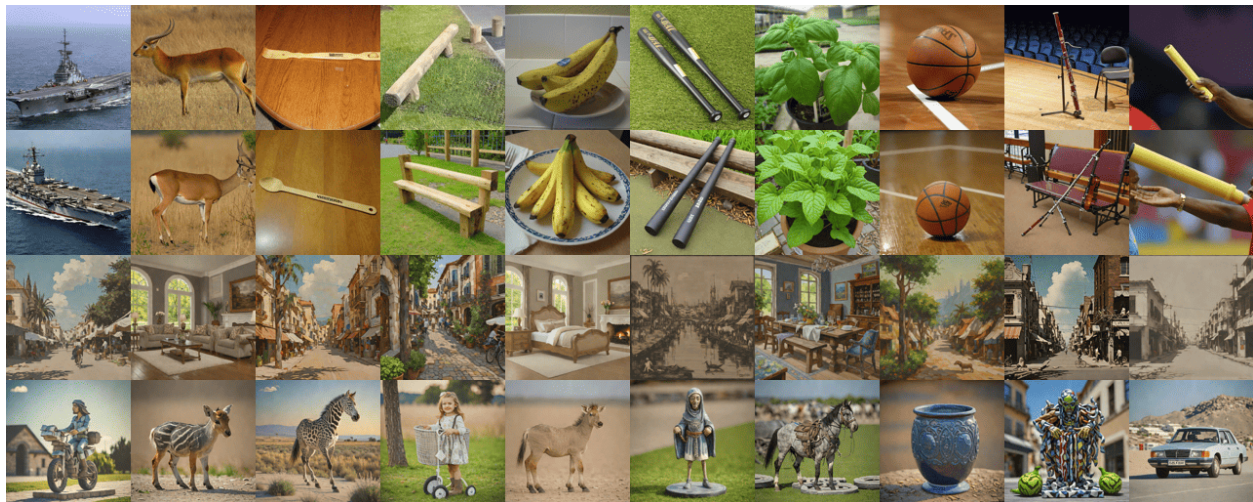


Figure 35: Random selected generated images in Subject 7 with ATM-S EEG encoder.

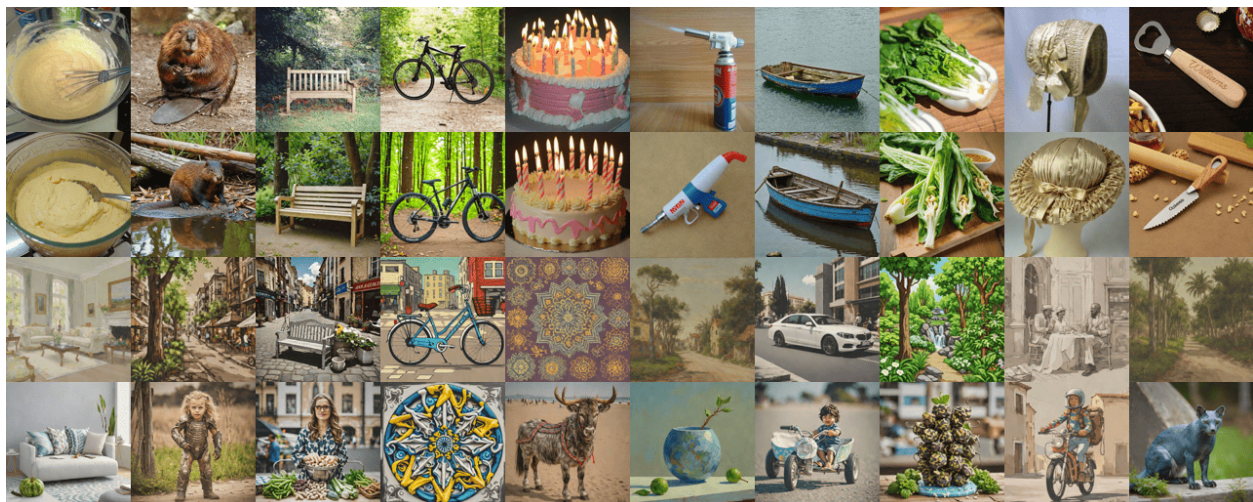


Figure 36: Random selected generated images in Subject 7 with ATM-S EEG encoder.



Figure 37: Random selected generated images in Subject 7 with ATM-S EEG encoder.

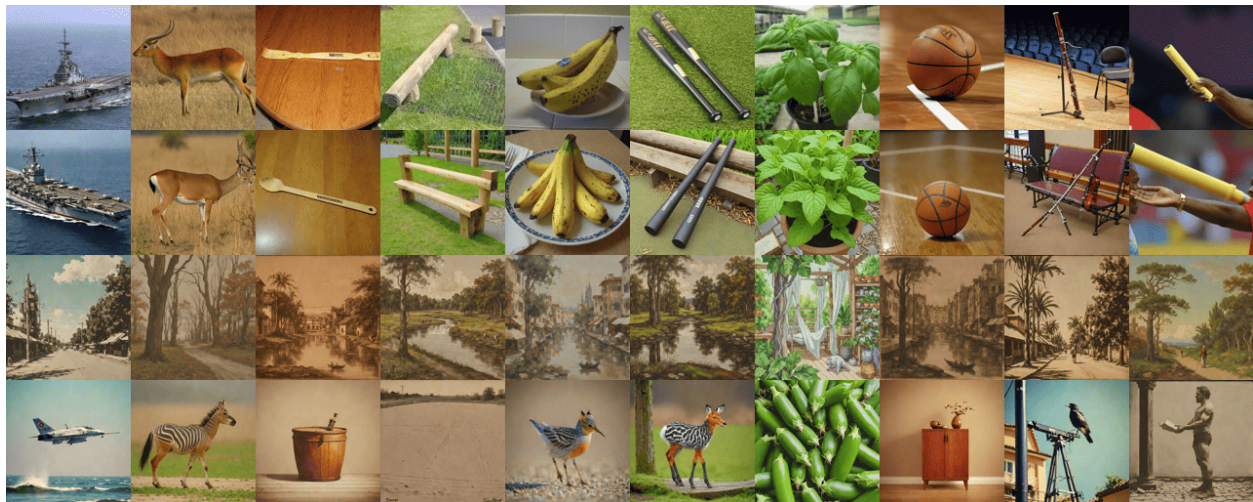


Figure 38: Random selected generated images in Subject 8 with ATM-S EEG encoder.



Figure 39: Random selected generated images in Subject 8 with ATM-S EEG encoder.

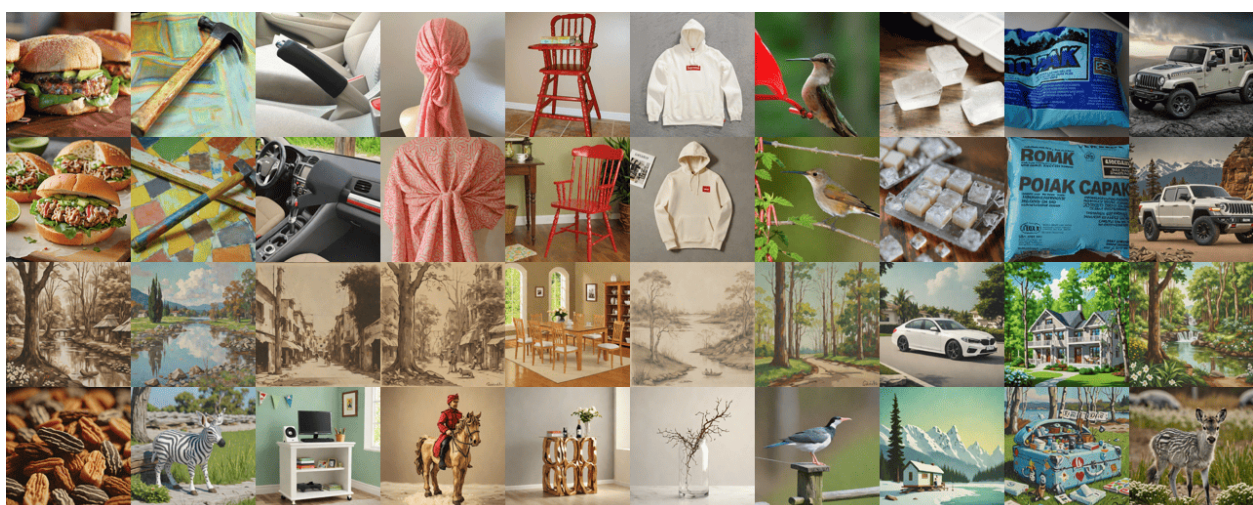


Figure 40: Random selected generated images in Subject 8 with ATM-S EEG encoder.

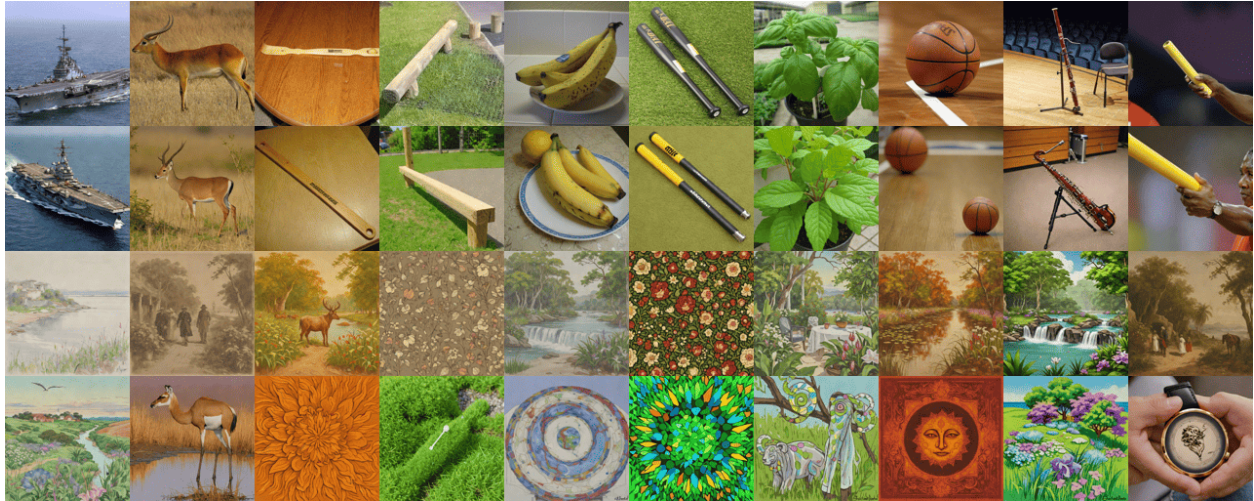


Figure 41: Random selected generated images in Subject 6 with NERV EEG encoder.

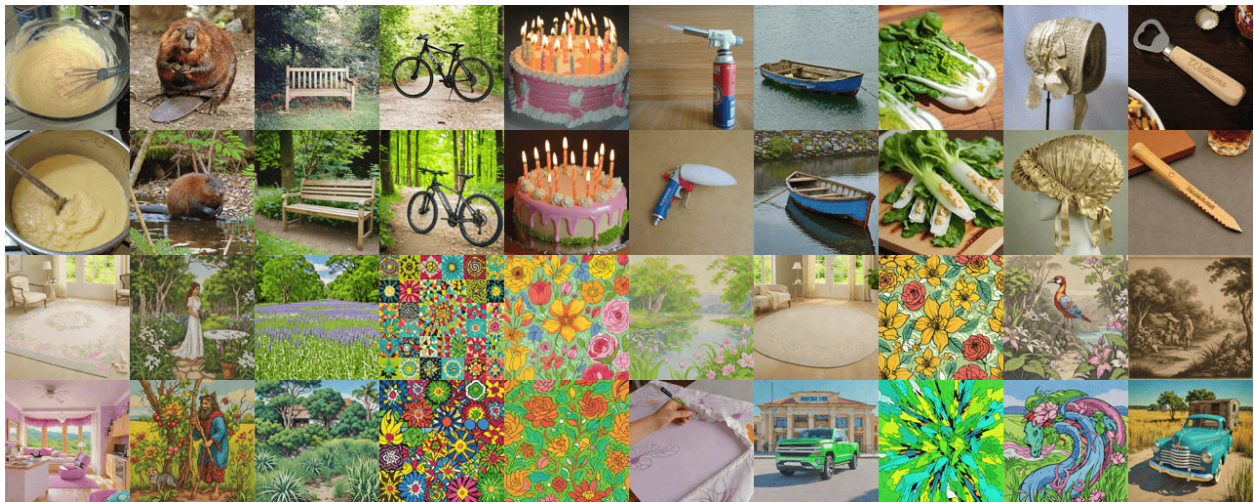


Figure 42: Random selected generated images in Subject 6 with NERV EEG encoder.

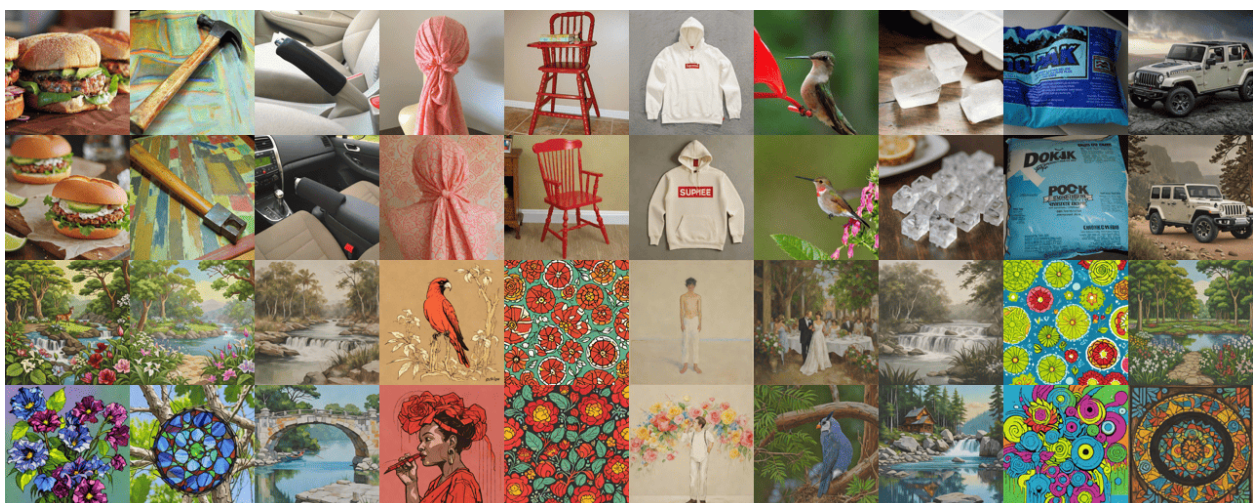


Figure 43: Random selected generated images in Subject 6 with NERV EEG encoder.



Figure 44: Random selected generated images in Subject 7 with NERV EEG encoder.



Figure 45: Random selected generated images in Subject 7 with NERV EEG encoder.



Figure 46: Random selected generated images in Subject 7 with NERV EEG encoder.



Figure 47: Random selected generated images in Subject 8 with NERV EEG encoder.

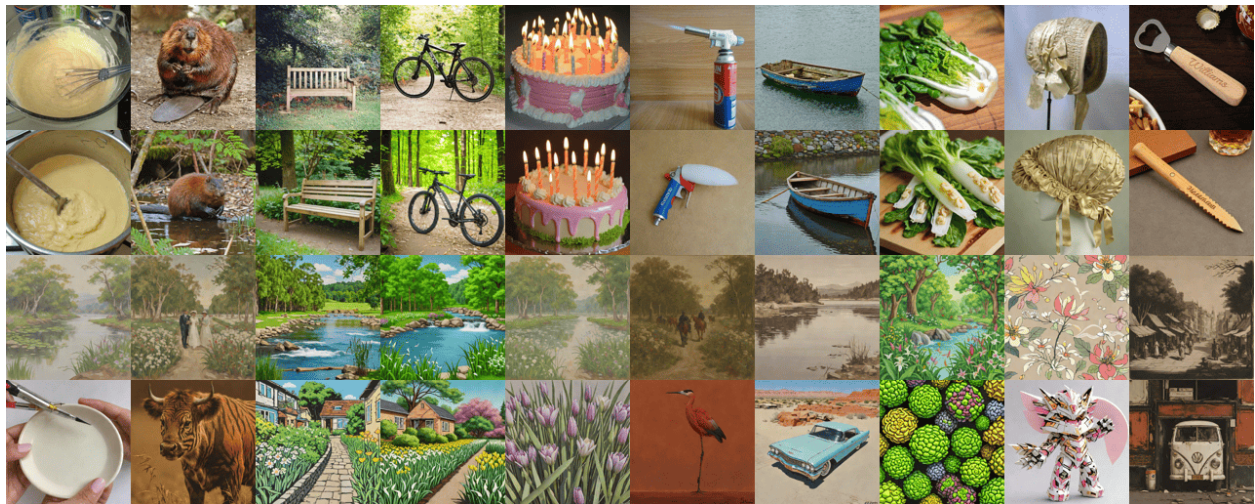


Figure 48: Random selected generated images in Subject 8 with NERV EEG encoder.

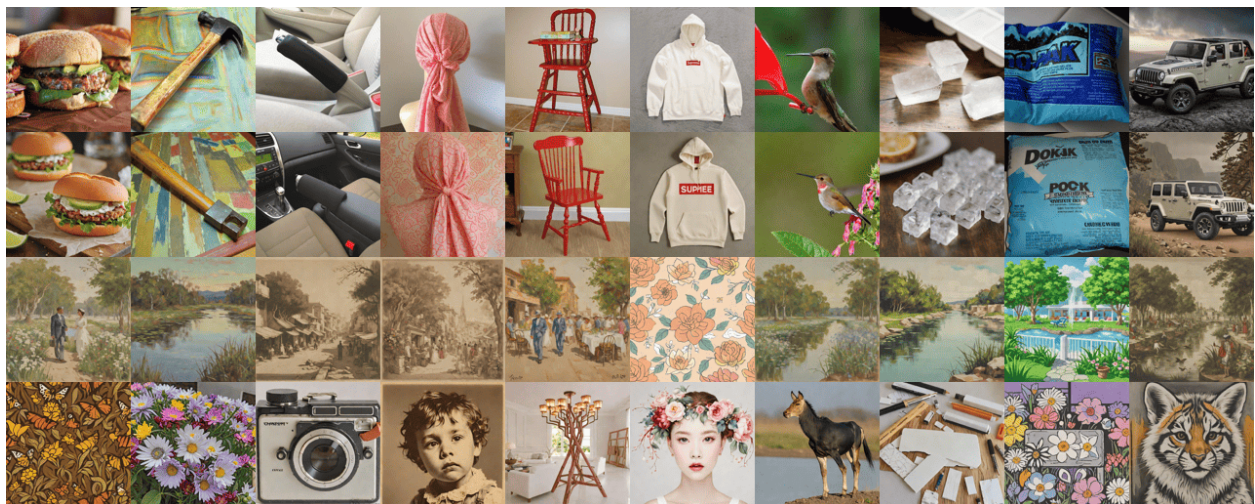


Figure 49: Random selected generated images in Subject 8 with NERV EEG encoder.